

Huygens' Metasurfaces for Antenna Applications



George V. Eleftheriades

The Edward S. Rogers, Sr. Department of Electrical
and Computer Engineering
University of Toronto
CANADA

29-Dec-16



ACKNOWLEDGEMENT

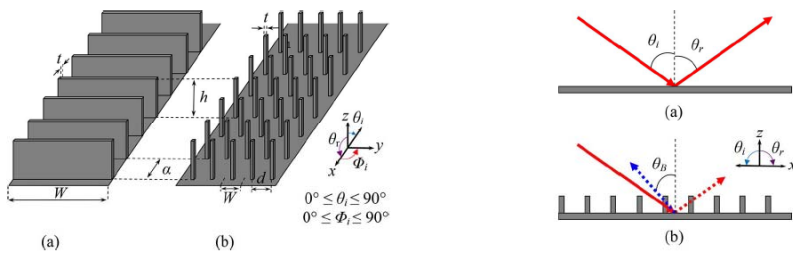
- Dr. Ariel Epstein
- Michael Selvanayagam
- Joseph Wong
- Trevor Cameron
- Michael Chen
- Alex Wong
- Min Kim

OVERVIEW

- Active Huygens' Metasurfaces for Cloaking
- Scalar Passive Huygens' Metasurfaces
- Refracting Metasurfaces
- Tensor and Chiral Huygens' Metasurfaces
- Shaping the Radiation of Closeby Sources
- Reflectionless Huygens' Metasurfaces
- Optical Metasurfaces
- Other Antenna Applications
- Summary

Stealth: Scattering re-direction

- Use shaped or engineered surfaces to reflect EM-waves in *non-specular* directions
- Examples:



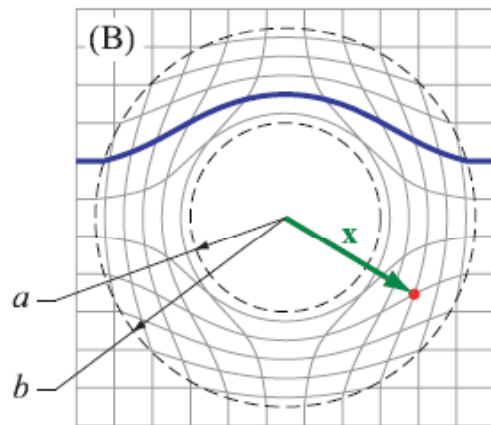
Davenport, C.J.; Rigelsford, J.M., "Specular Reflection Reduction Using Periodic Frequency Selective Surfaces," *Antennas and Propagation, IEEE Transactions on*, vol.62, no.9, pp.4518,4527, Sept. 2014



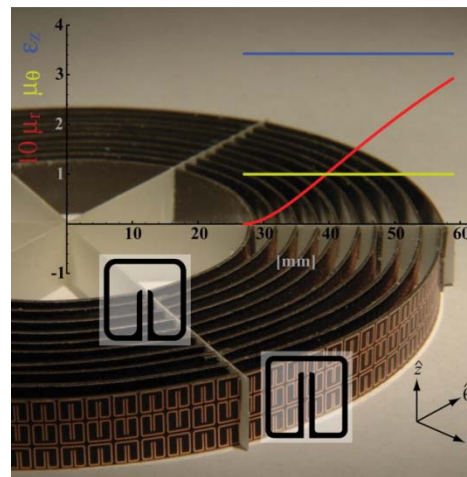
Can be detected with multistatic radar

METAMATERIAL CLOAKING

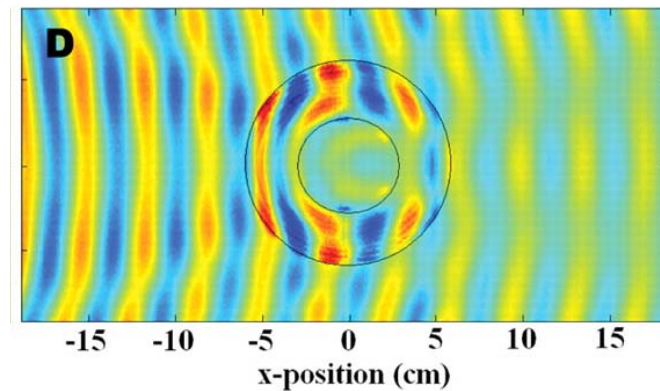
Transformation:



Fabrication:



Measurement:

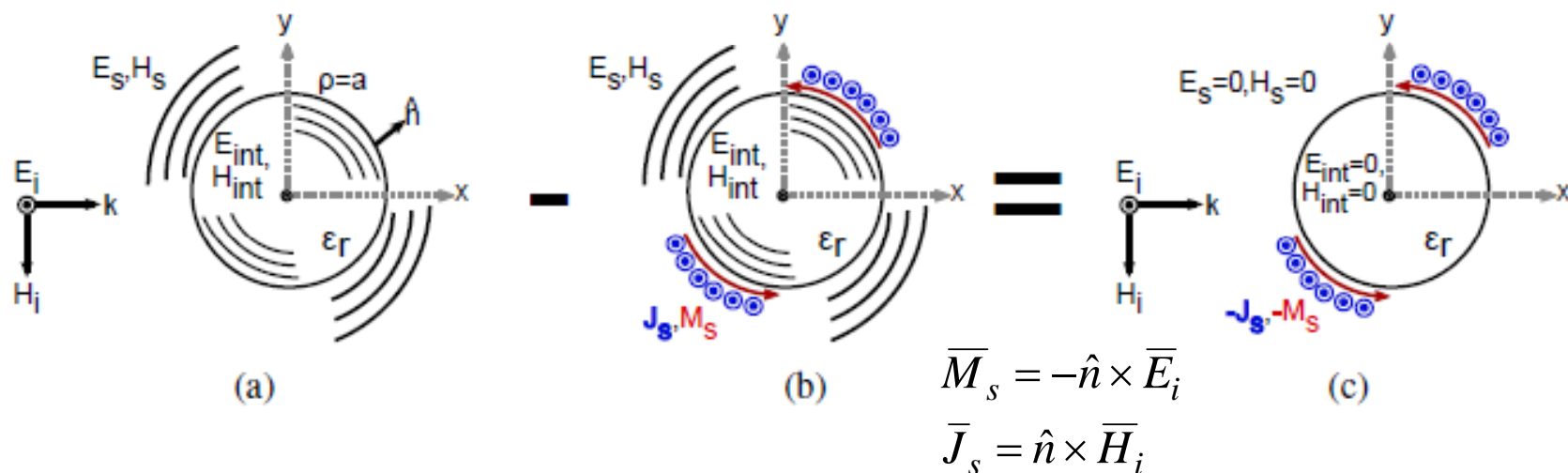


However cloak too bulky on the order of the size of the object

D. Schurig, J. J. Mock, B. J. Justice, S. A. Cummer, J. B. Pendry, A. F. Starr, and D. R. Smith, "Metamaterial Electromagnetic Cloak at Microwave Frequencies," *Science*, vol. 314, no. 5801, pp. 977–980, 2006.

ACTIVE CLOAKING

(equivalence principle)

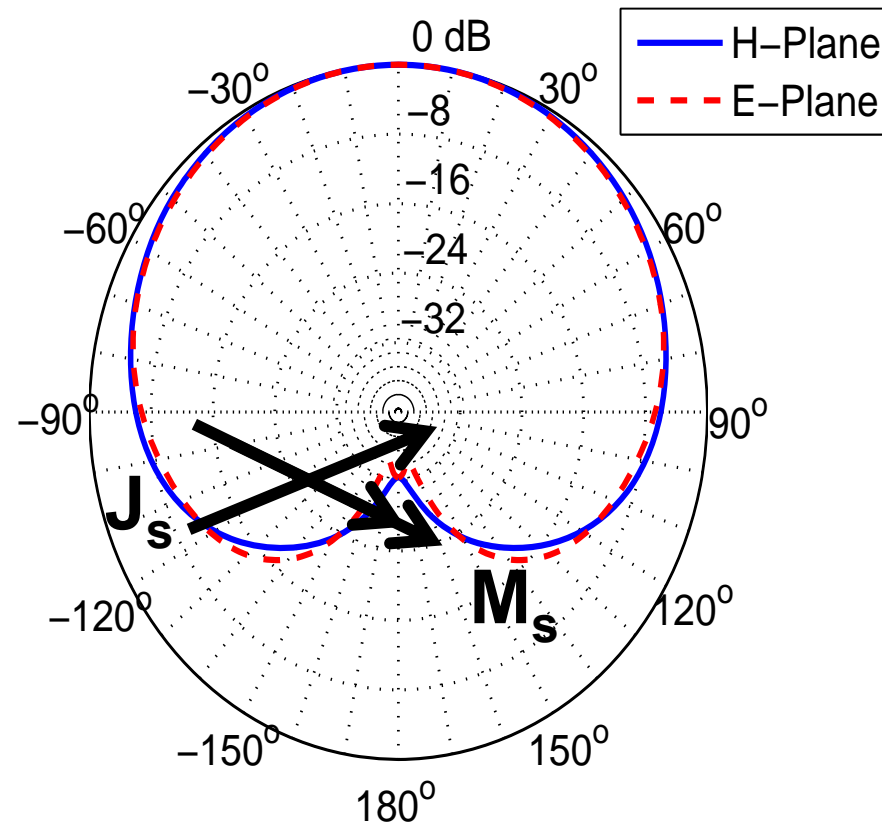


(a) Scattering of a plane wave off of a cylindrical object.

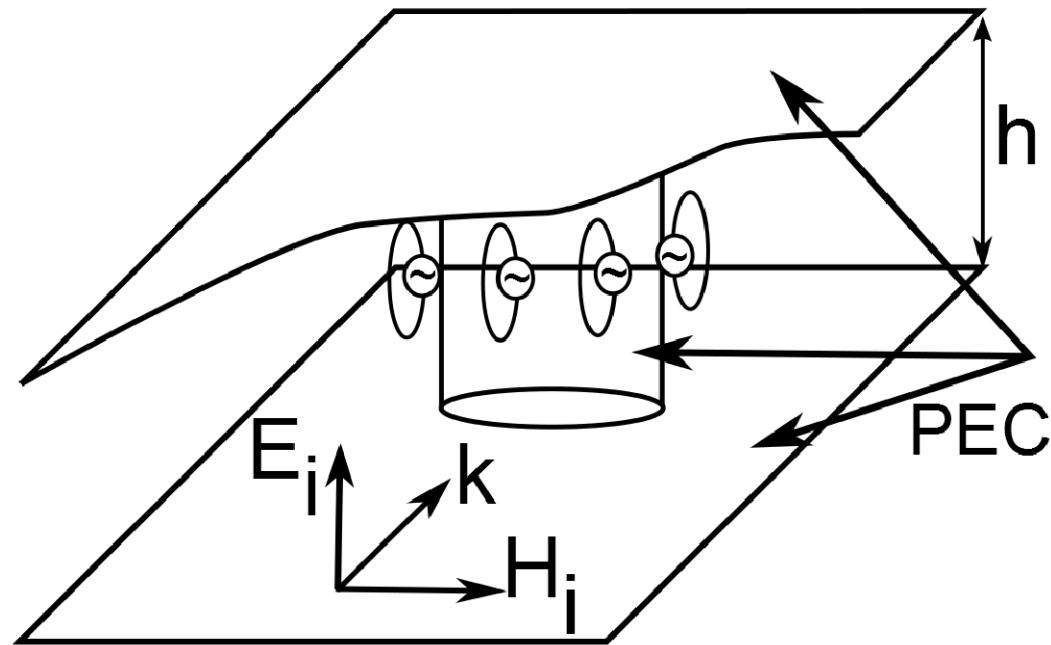
(b) An equivalent scenario where electric and magnetic current densities on the surface of the cylindrical object radiate the scattered field

(c) The superposition of (a) and (b) such that the scattered and interior fields are cancelled out.

Huygens' Source Unit Cells



ACTIVE CLOAKING

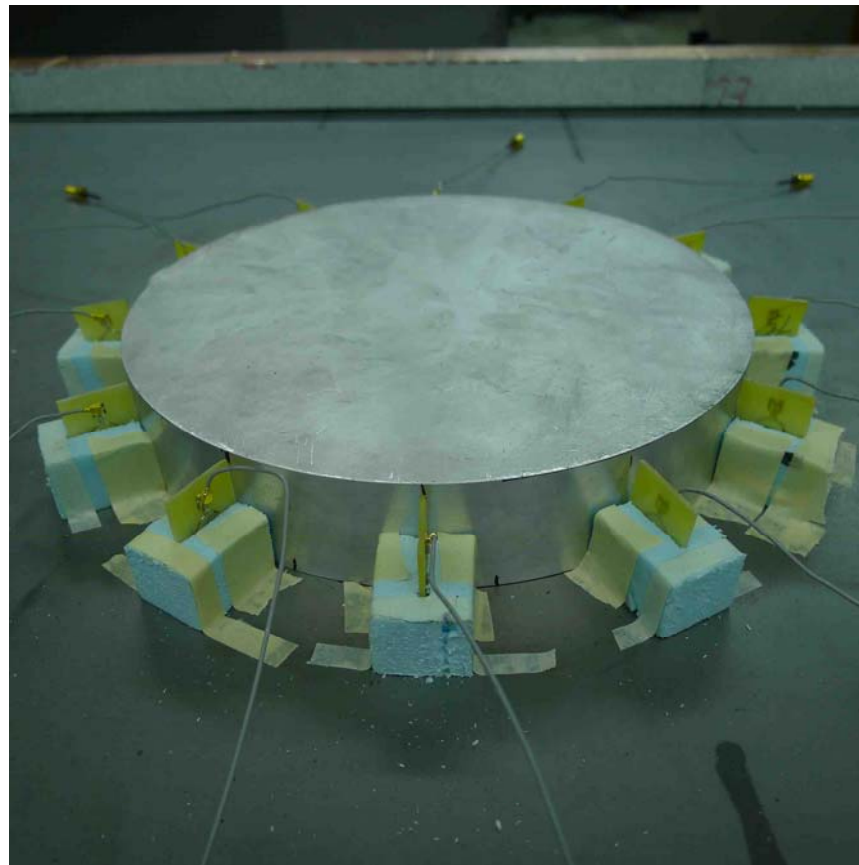


Just surround a (say) metal cylinder with magnetic dipoles (loop antennas) to create a magnetic current that cancels out the scattered field.

Cloaking

Cloak Design

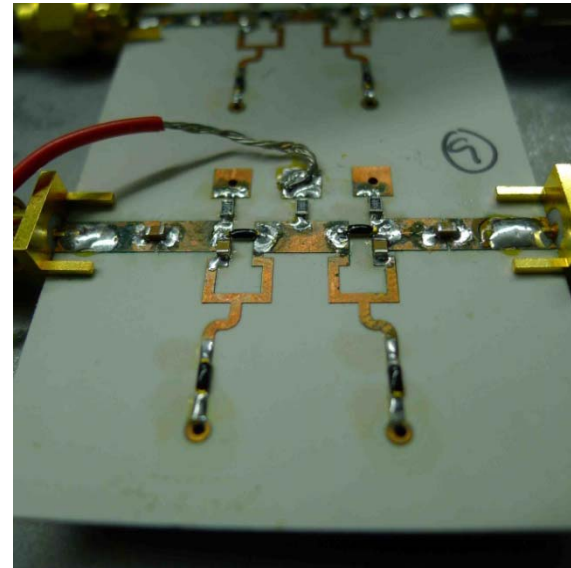
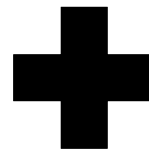
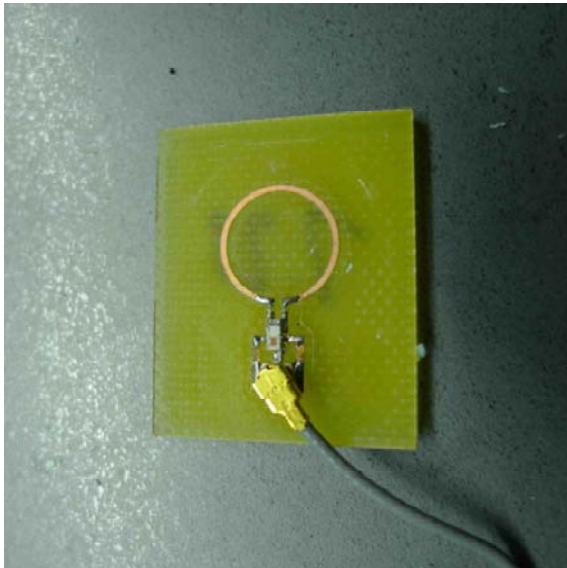
- 12 total small loops to form an array



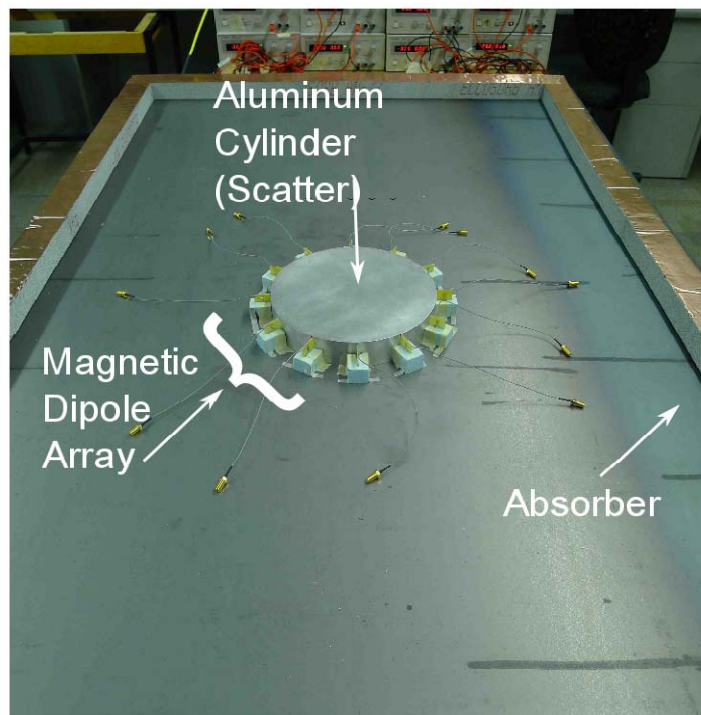
Cloaking

Cloak Design

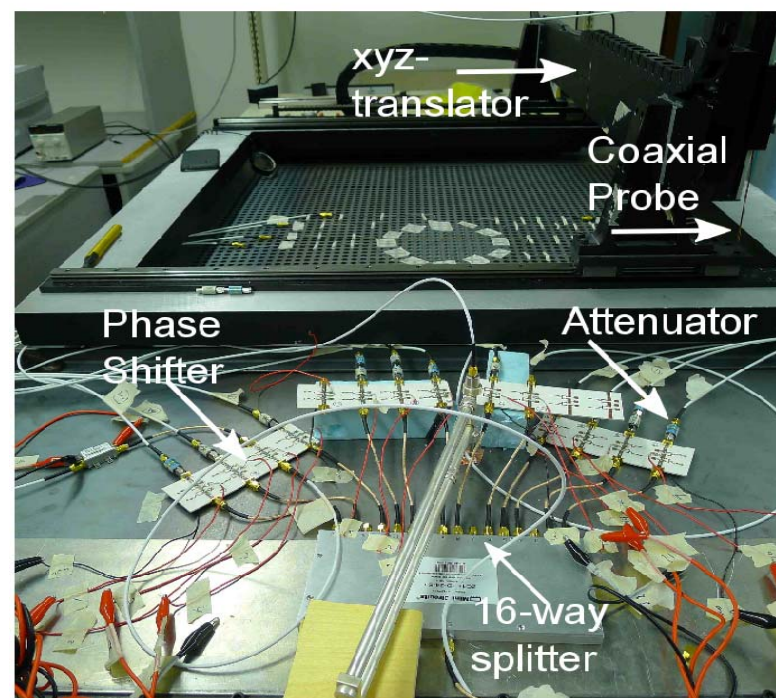
- Cloak consists of loop antennas (magnetic dipoles)
- Fed through phase shifters (outside waveguide)



Measurement Setup



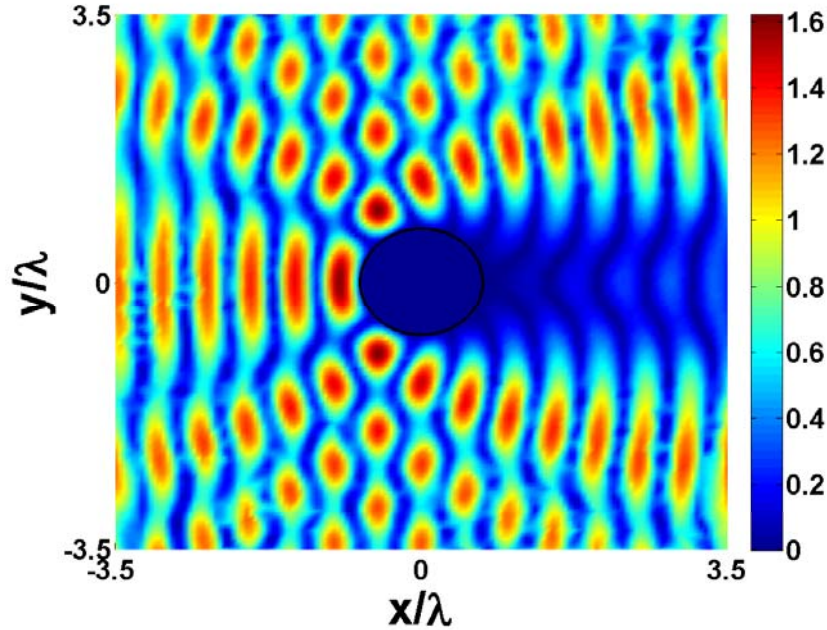
Inside Waveguide



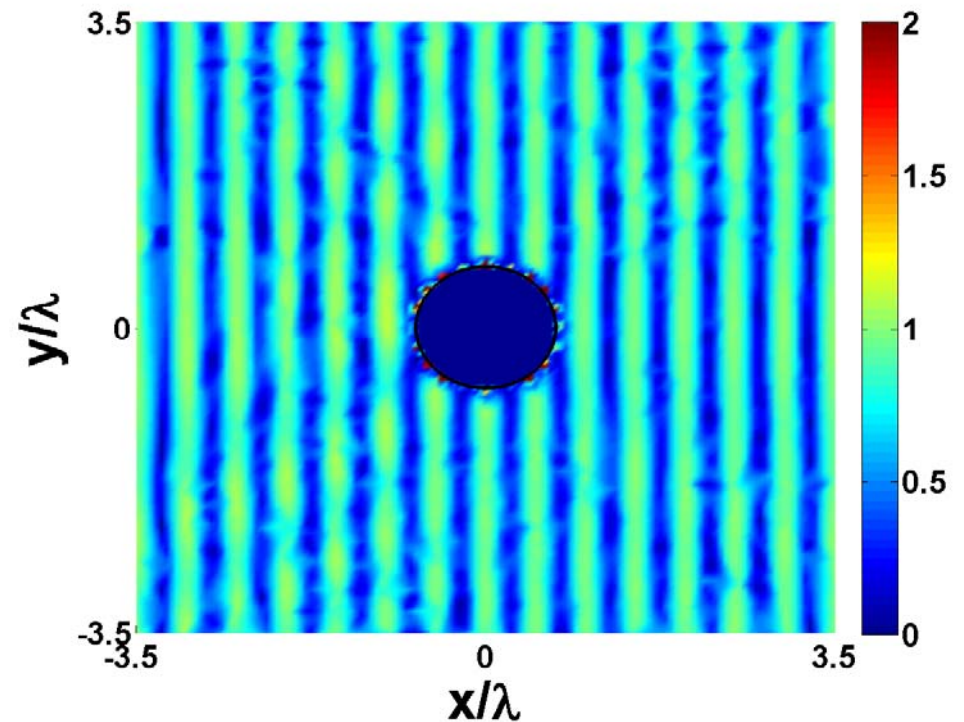
Outside Waveguide

Fullwave Simulation

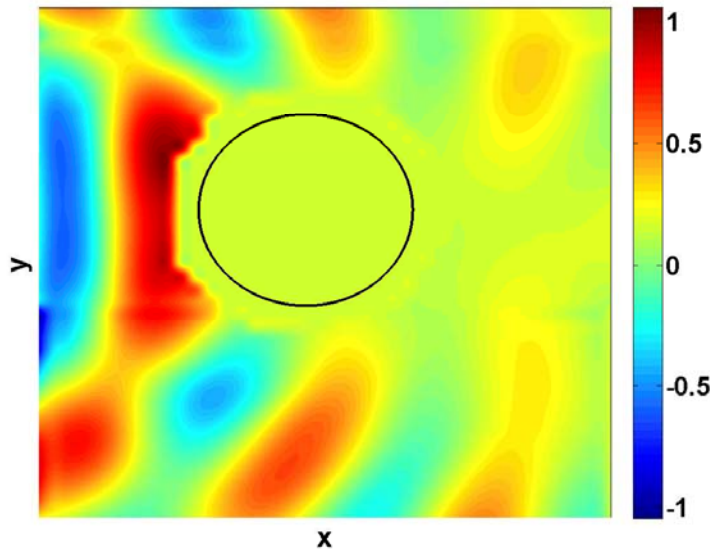
Without active cloak



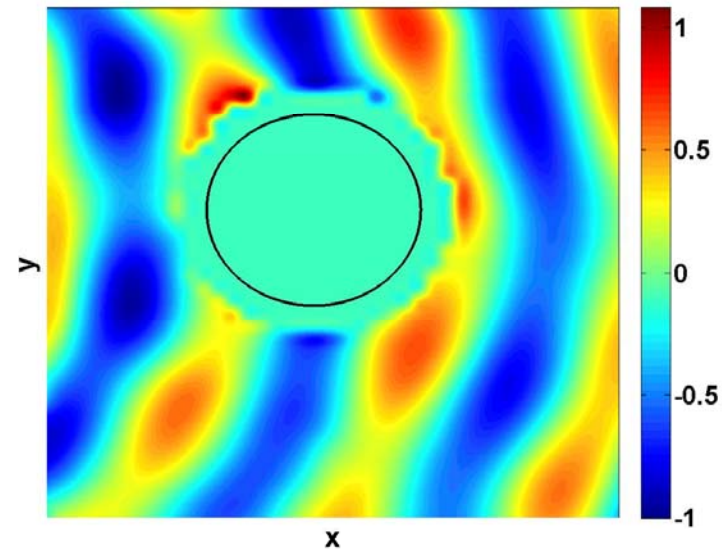
With active cloak



Measured

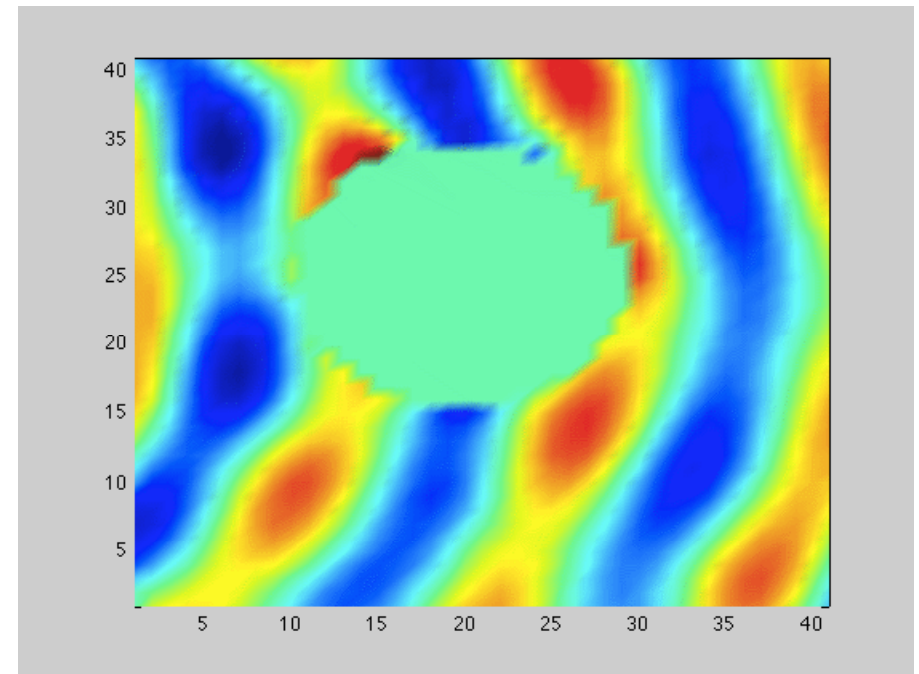
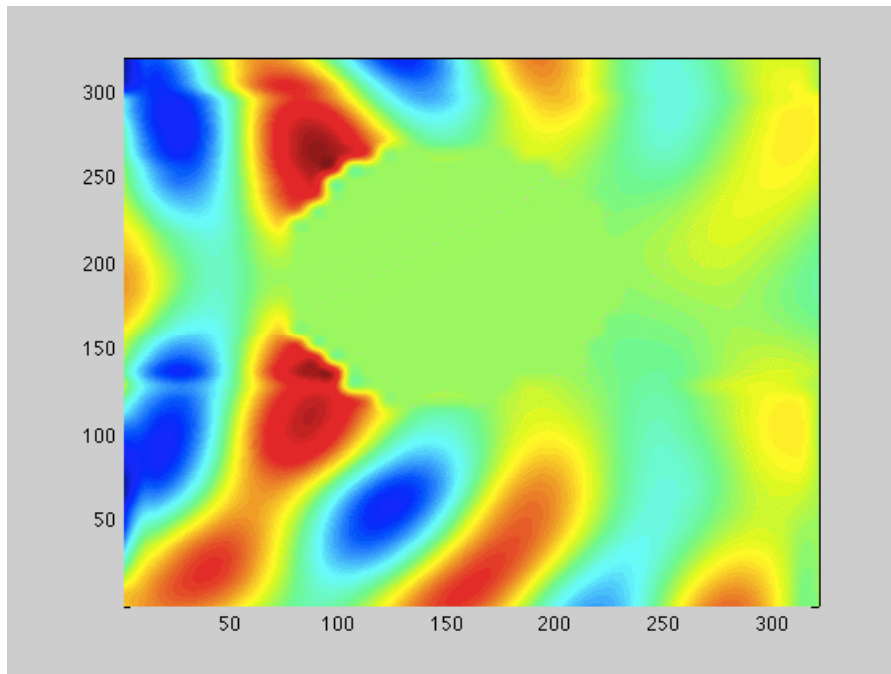


Measured Fields:
Scattering off of a
metallic cylinder.
Note the shadow
region



Measured Cloak: note
that the wavefronts
now pass around the
cylinder as if it was
not there

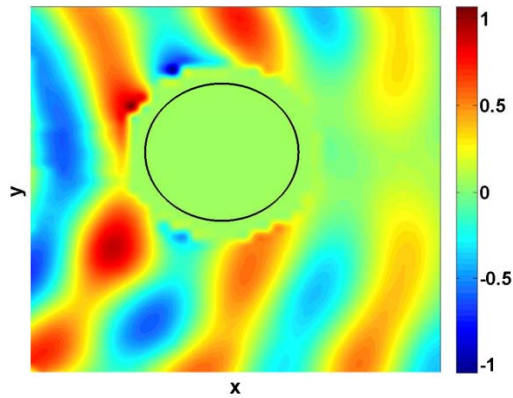
Cloaking: Measured Waves



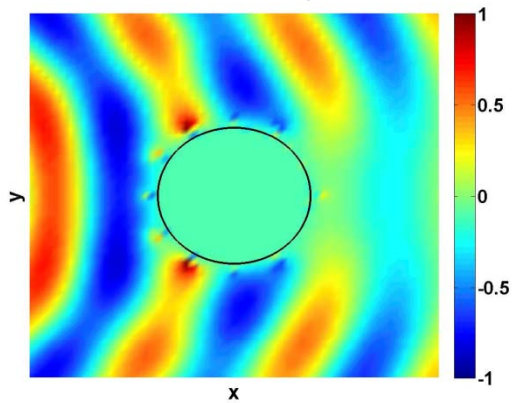
Camouflage Results



Small Metallic Cylinder Disguise

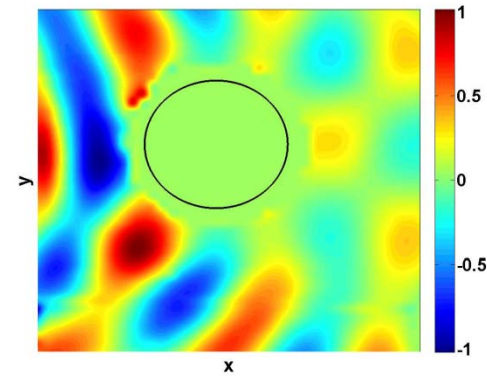


Measured Scattering off of disguised cylinder. Note the smaller shadow region

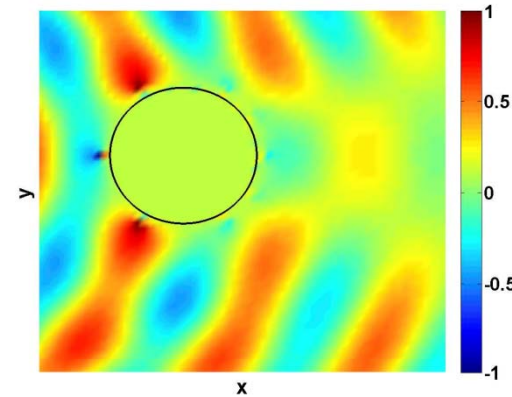


Simulated dielectric cylinder (COMSOL)

Dielectric Cylinder Disguise

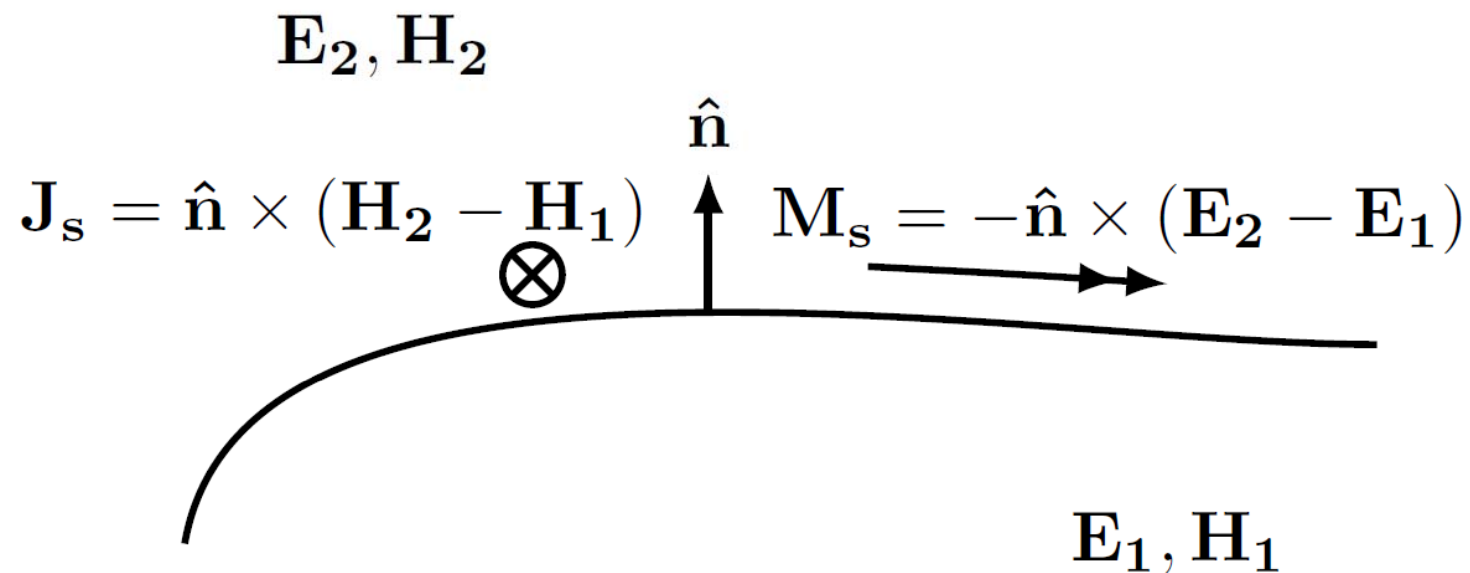


Measured Scattering off of disguised cylinder. Note how the shadow regions has been modified



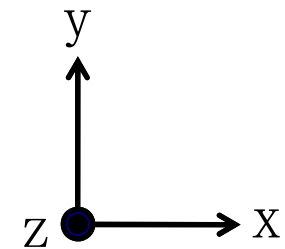
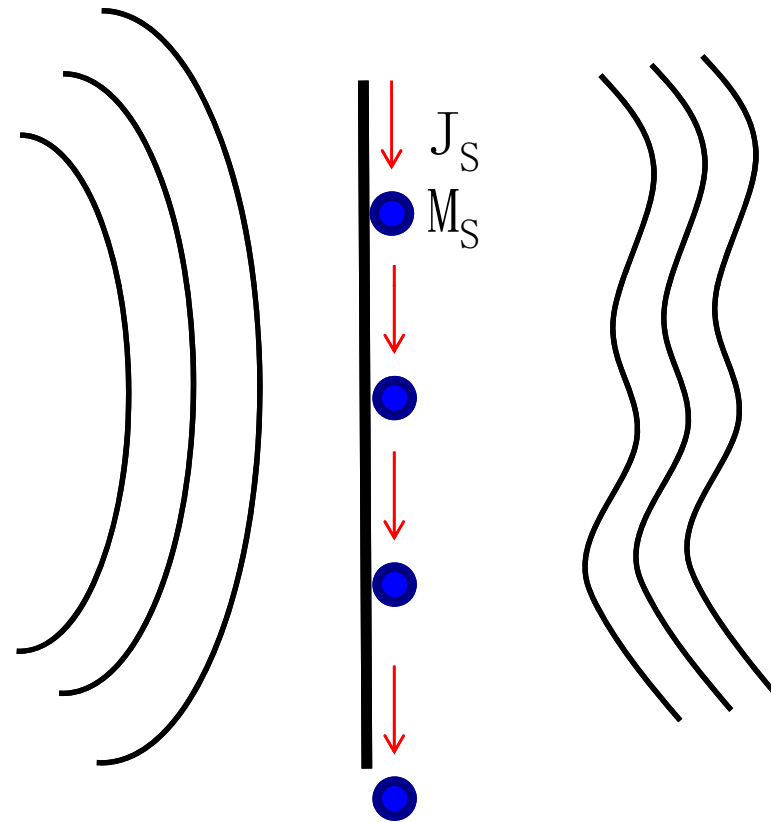
Simulated smaller cylinder (COMSOL)

Huygens' Metasurface Description (equivalence principle)

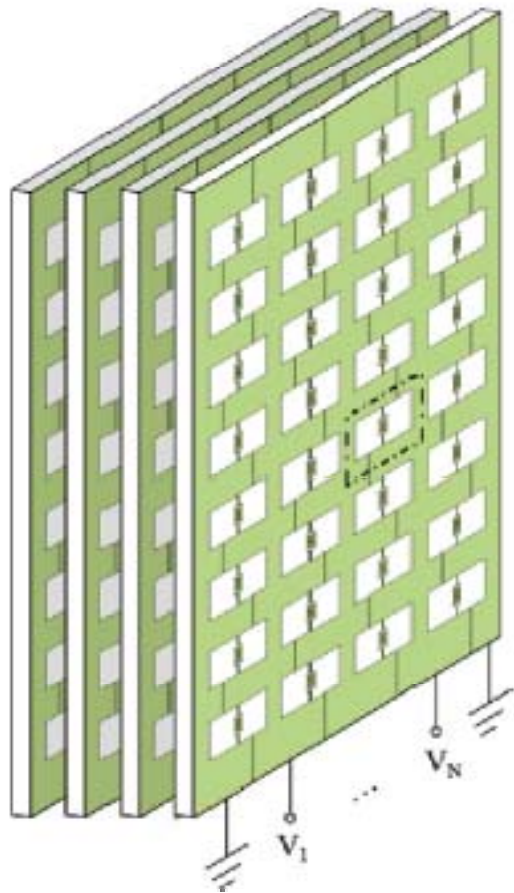


- [1] M. Selvanayagam and G.V. Eleftheriades, *Optics Express*, 2013
[2] C. Pfeiffer and A. Grbic, *Physical Review Letters*, 2013

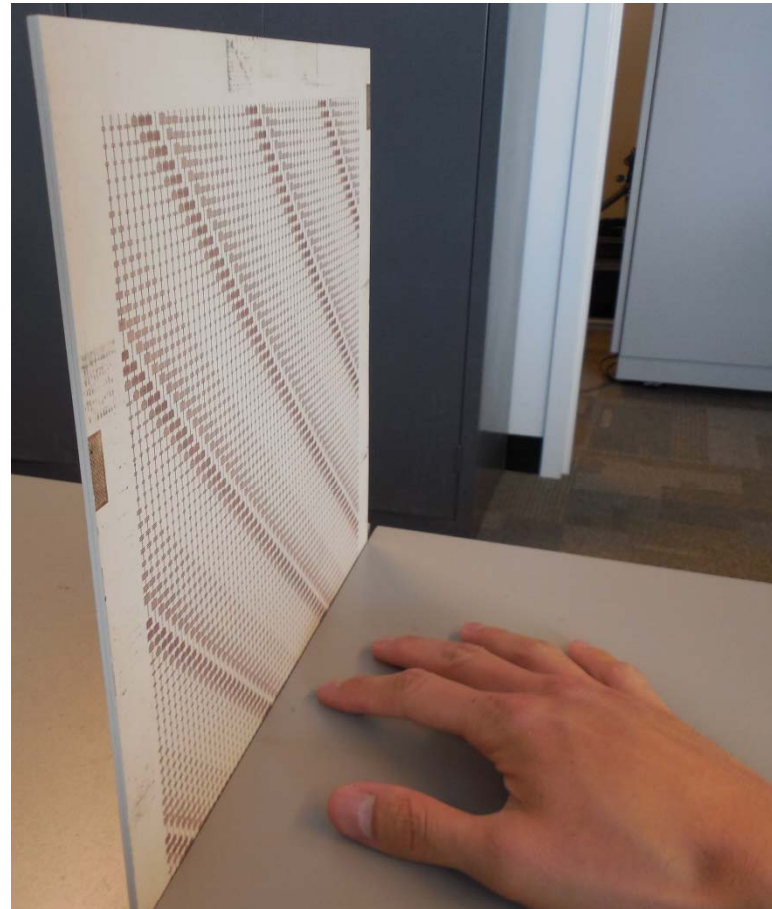
Wavefront Shaping



Motivation: Thin Surfaces for Complete EM-control (magnitude, phase, polarization; no or small reflections)



Traditional Transmit-array



Thin ($\lambda/10$) Huygens' metasurface
No spurious Floquet modes



Huygens' Metasurface Description

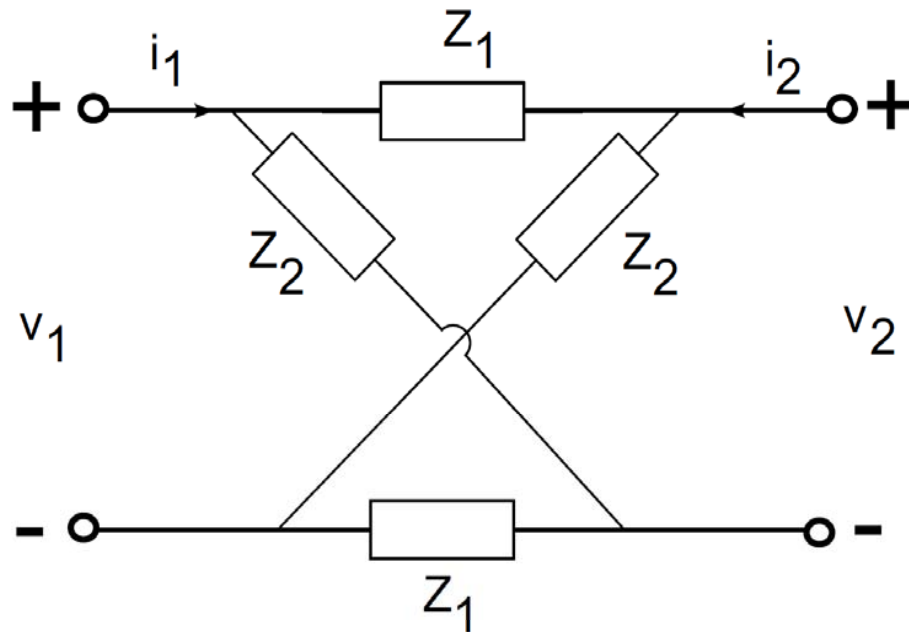
Impedance Boundary Condition:

$$\left. \frac{\mathbf{E}_2 + \mathbf{E}_1}{2} \right|_{\text{tan.}} = X_{\text{se}} \hat{\mathbf{n}} \times (\mathbf{H}_2 - \mathbf{H}_1)$$

Admittance Boundary Condition:

$$\left. \frac{\mathbf{H}_2 + \mathbf{H}_1}{2} \right|_{\text{tan.}} = B_{\text{sm}} \hat{\mathbf{n}} \times (\mathbf{E}_2 - \mathbf{E}_1)$$

Lattice Network Model



Impedances:

$$Z_1 = -jB_{sm}^{-1} = 2(Z_{11} - Z_{21})$$

$$Z_2 = jX_{se} = \frac{Z_{11} + Z_{21}}{2}$$

Circuit Equations:

$$I_1 + I_2 = (1/Z_1)(V_1 - V_2)$$

$$V_1 + V_2 = Z_2(I_1 - I_2)$$

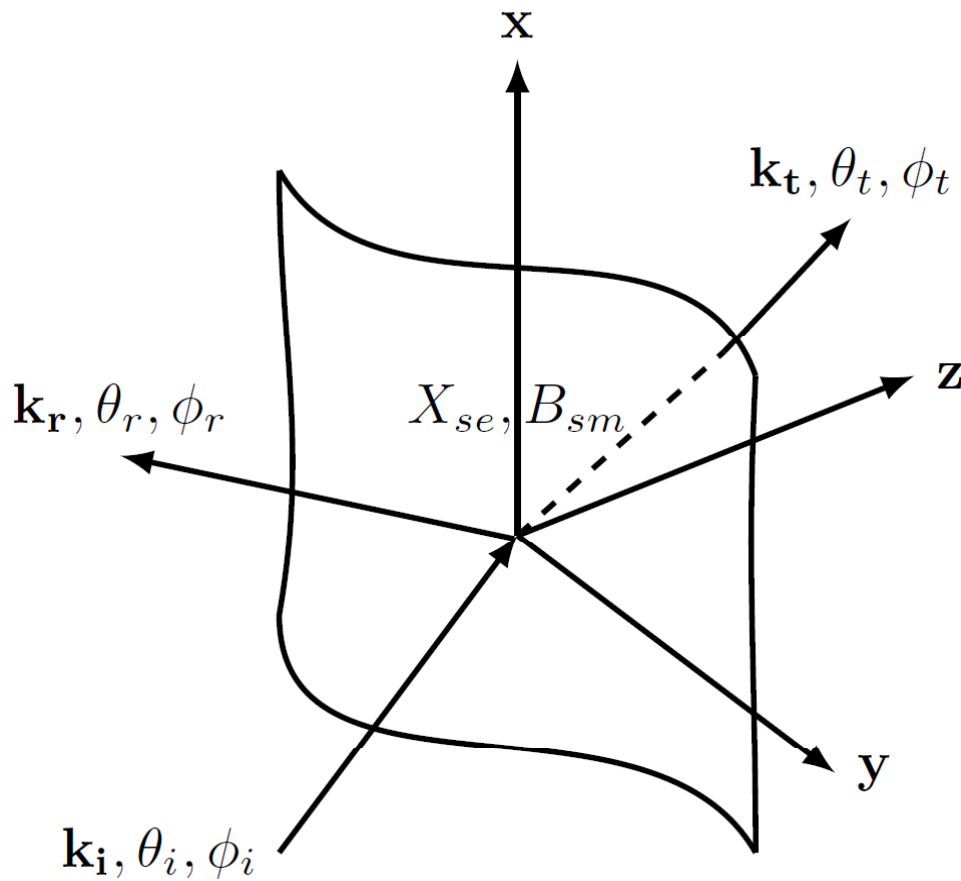
Field Boundary Cond.:

$$\left. \frac{\mathbf{H}_2 + \mathbf{H}_1}{2} \right|_{\text{tan.}} = B_{sm} \hat{\mathbf{n}} \times (\mathbf{E}_2 - \mathbf{E}_1)$$

$$\left. \frac{\mathbf{E}_2 + \mathbf{E}_1}{2} \right|_{\text{tan.}} = X_{se} \hat{\mathbf{n}} \times (\mathbf{H}_2 - \mathbf{H}_1)$$



2D Refraction



$$\begin{aligned}\mathbf{E}_{\text{inc}} &= E_{0\text{inc}} e^{-j\mathbf{k}_{\text{inc}} \cdot \mathbf{r}} \\ \mathbf{E}_{\text{refl}} &= E_{0\text{refl}} e^{-j\mathbf{k}_{\text{refl}} \cdot \mathbf{r}} \\ \mathbf{E}_{\text{refr}} &= E_{0\text{refr}} e^{-j\mathbf{k}_{\text{refr}} \cdot \mathbf{r}}\end{aligned}$$



Impedance and Admittance Spatial Profile

Electric Impedances:

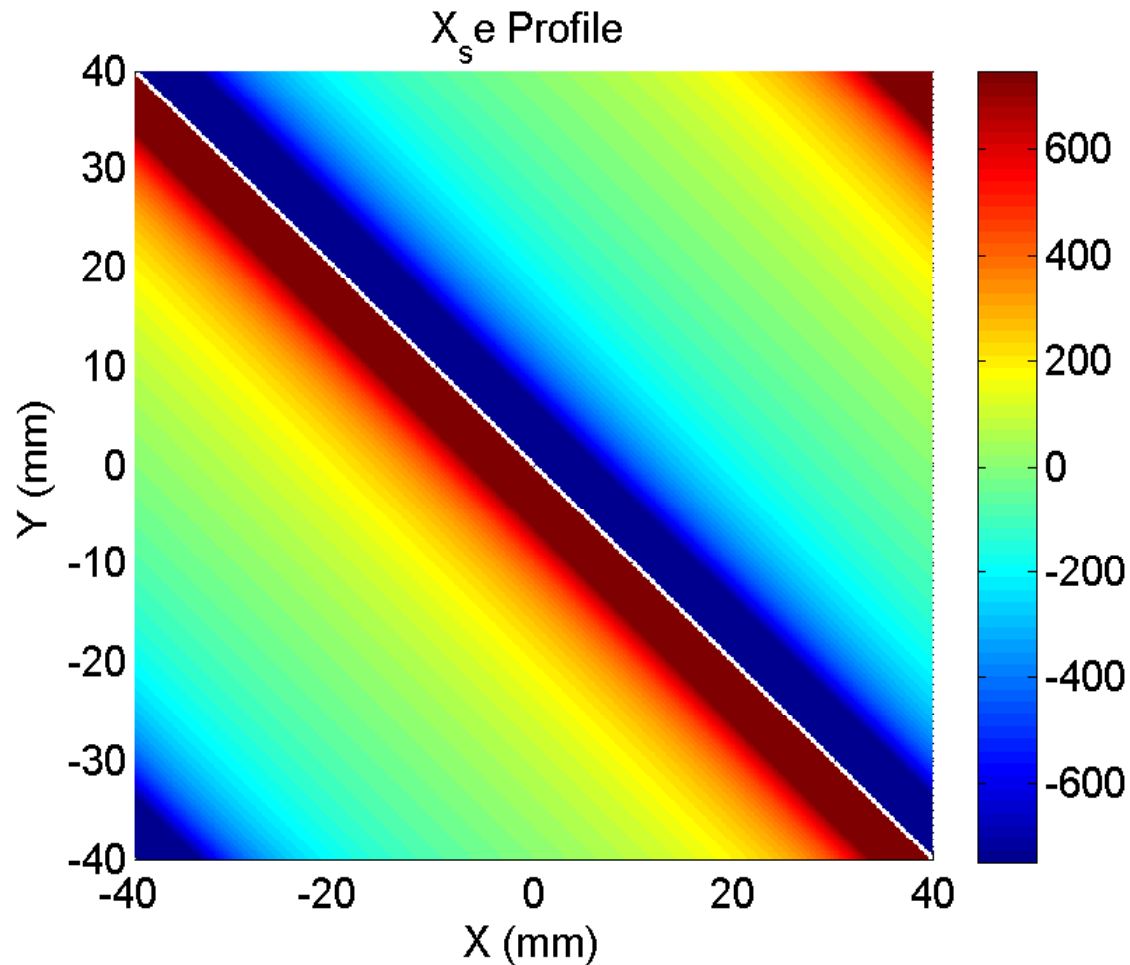
$$X_{se} = -\frac{\eta}{2 \cos(\theta_i)} \cot(\Phi/2)$$

Magnetic Admittances:

$$B_{sm} = -\frac{\cos(\theta_t)}{2\eta} \cot(\Phi/2)$$

$$\Phi = (\mathbf{k}_t - \mathbf{k}_i) \cdot \mathbf{r}$$

2D Impedance X_{se} Profile



■ Design Specs:

□ 10 GHz

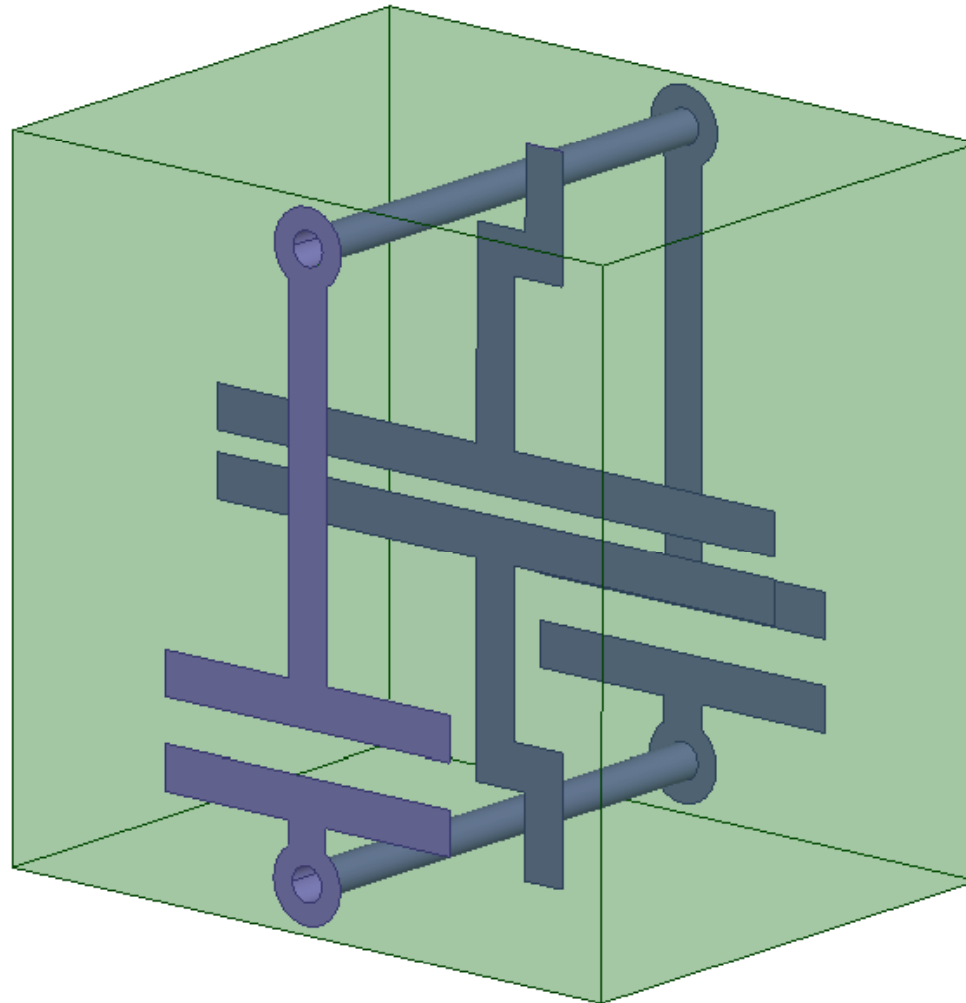
□ $\theta_i = 0^\circ$

□ $\varphi_i = 0^\circ$

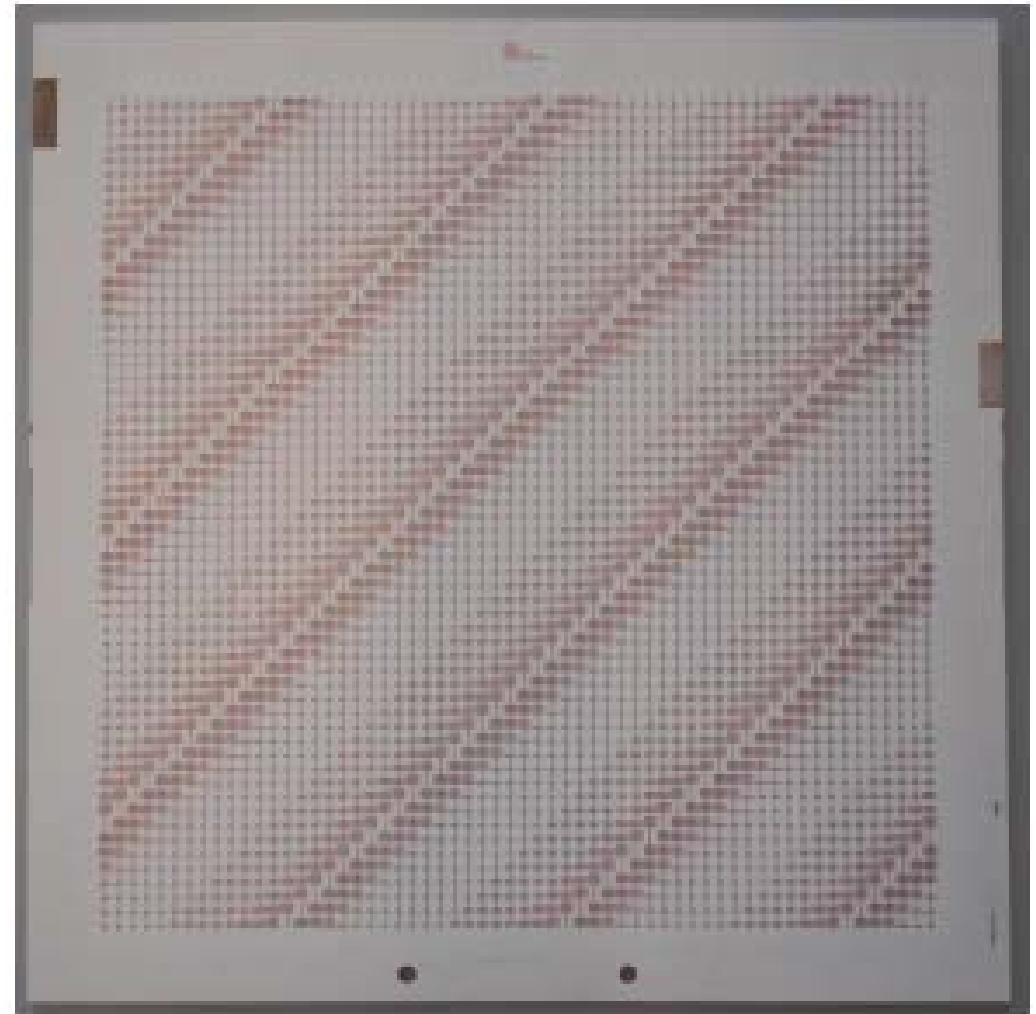
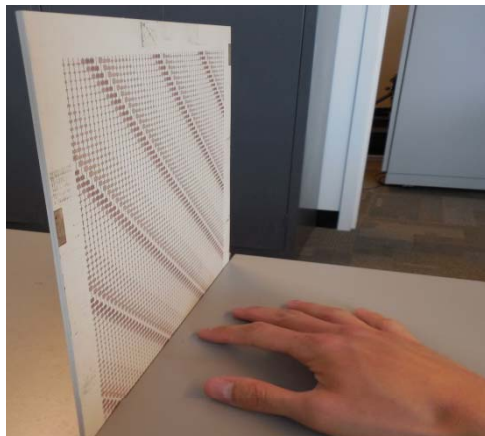
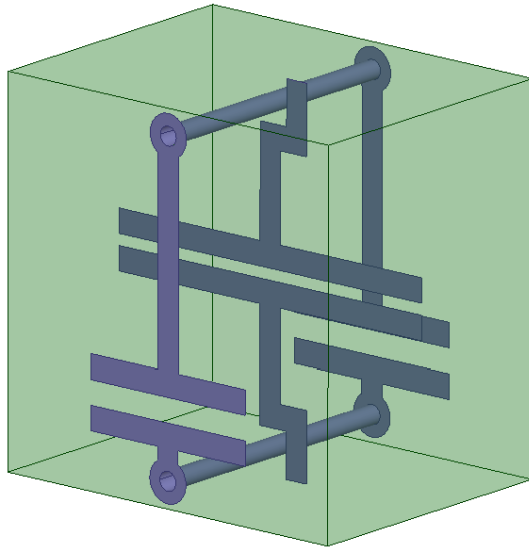
□ $\theta_t = 32.08^\circ$

□ $\varphi_t = 45.00^\circ$

Unit-Cell Geometry

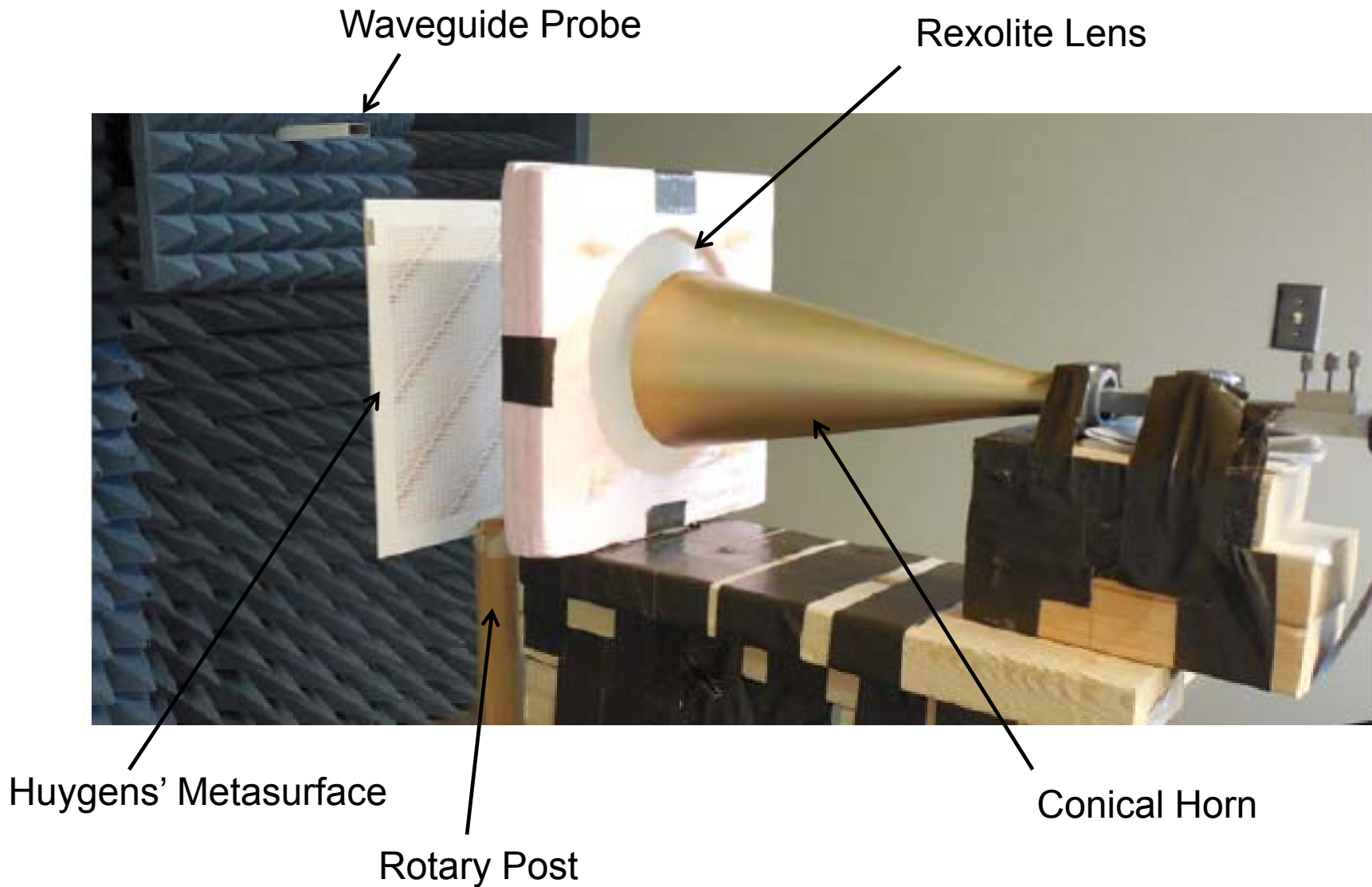


A 2D-Refractive Metasurface

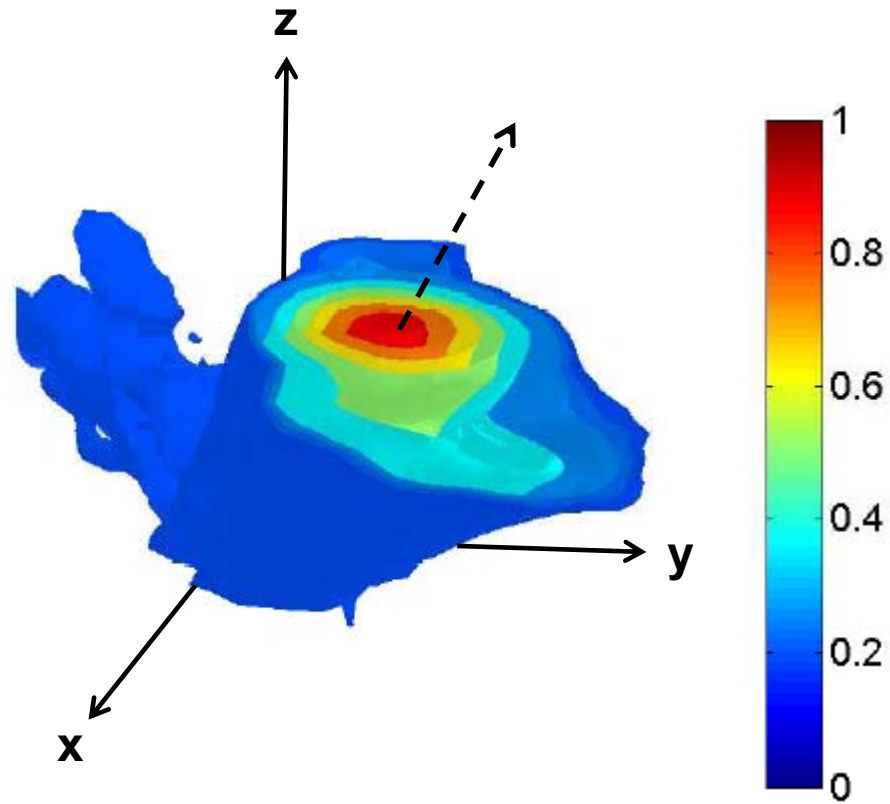


J.P.S. Wong, M. Selvanayagam and G.V. Eleftheriades, "Characterization of Huygens metasurfaces for 2D refraction", *IEEE Trans. on Microwave Theory and Techn.*, 2015.

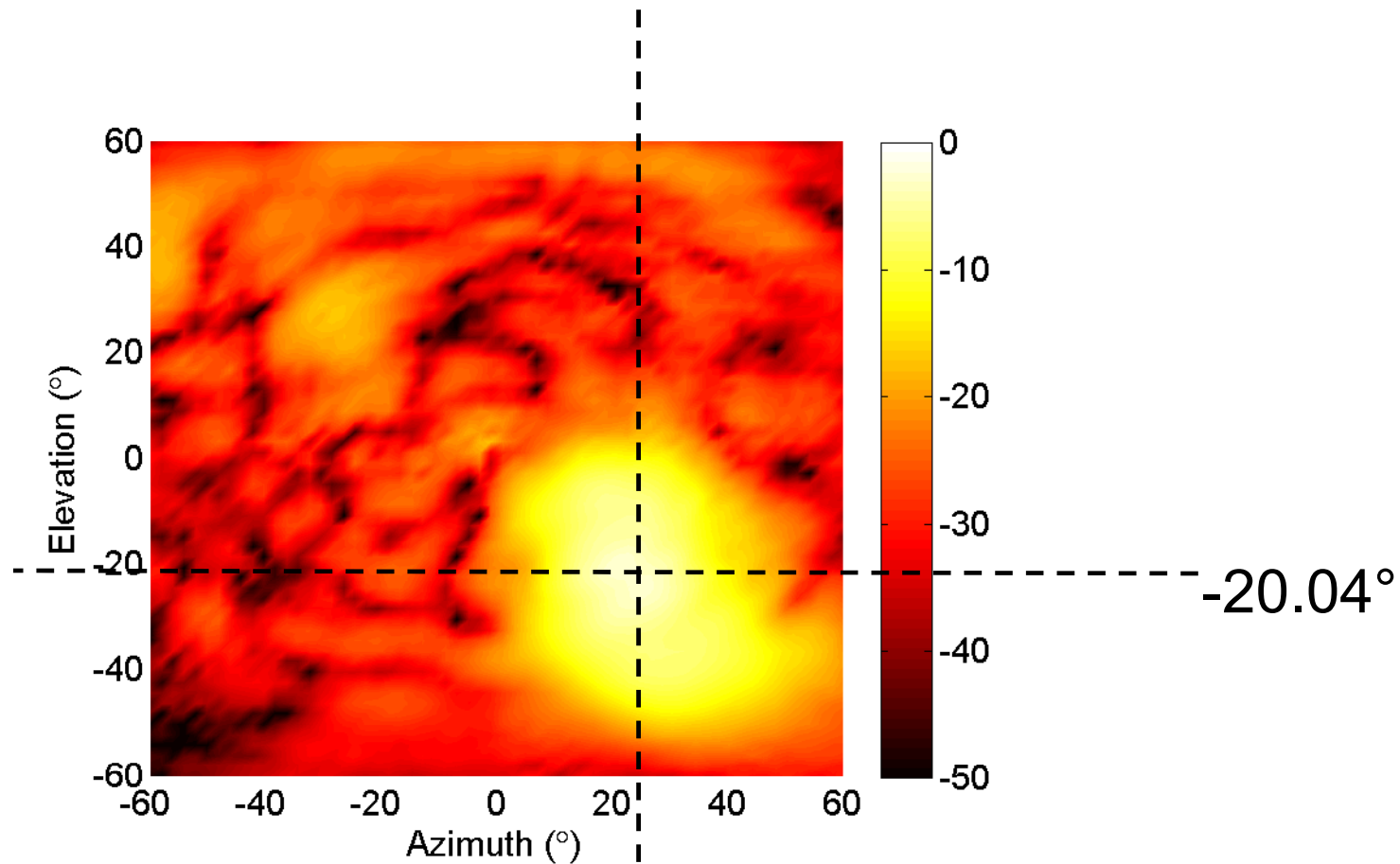
Experimental Setup



Near-Field Isosurfaces



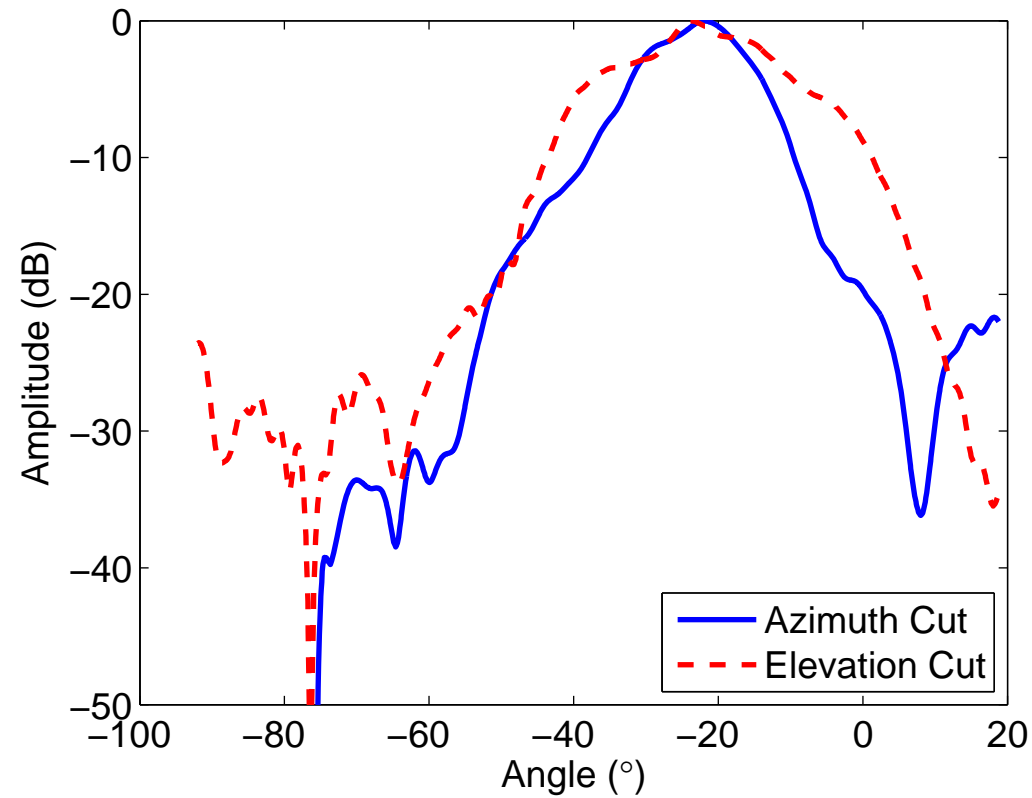
Far-Field Pattern



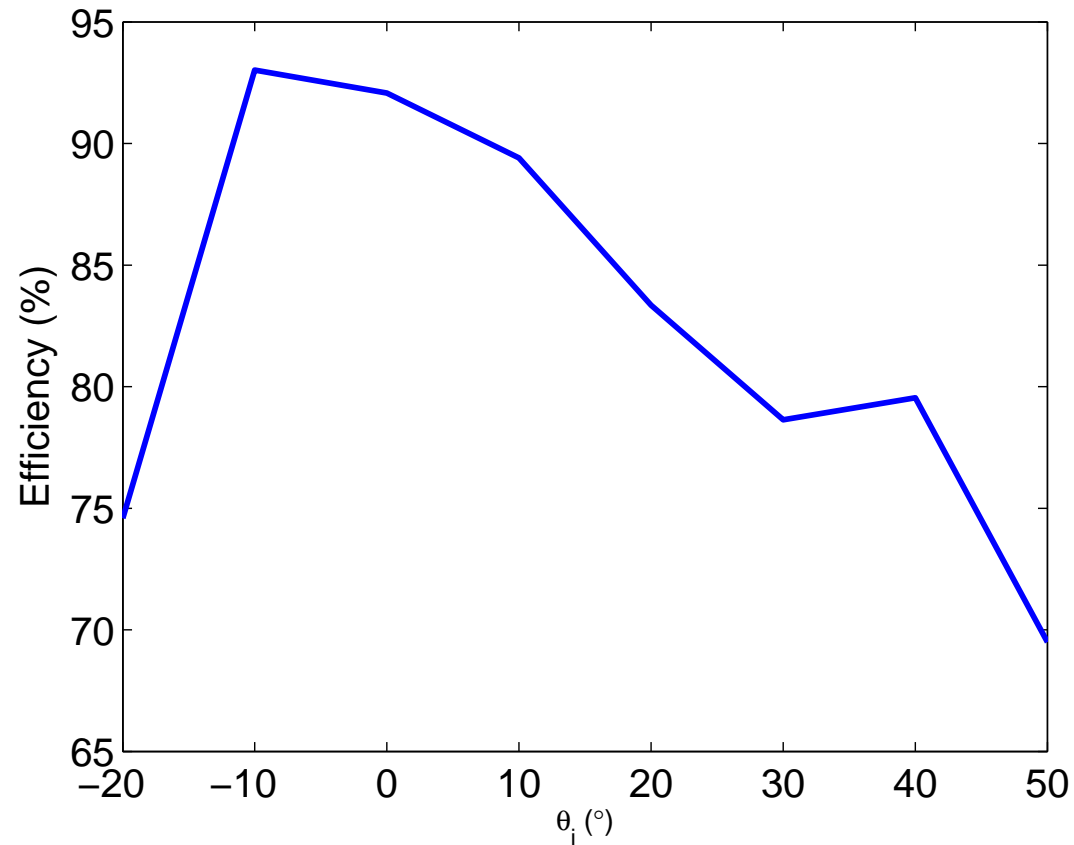
(Azimuth = 21.83°, Elevation = -20.04°) \Leftrightarrow ($\theta=29.29^\circ$ $\varphi=-44.45^\circ$)
21.83°



Far-Field Pattern Cuts @ 10GHz

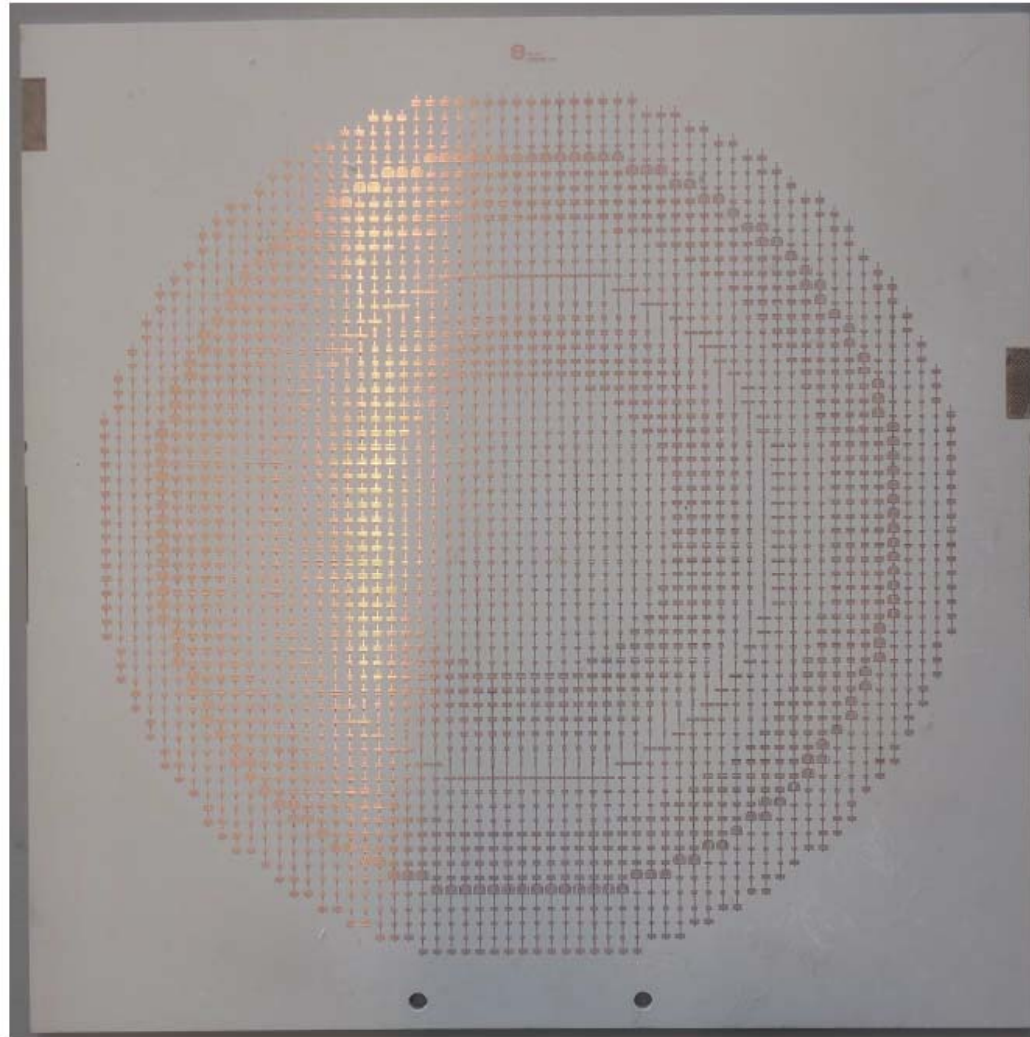


Measured Efficiency

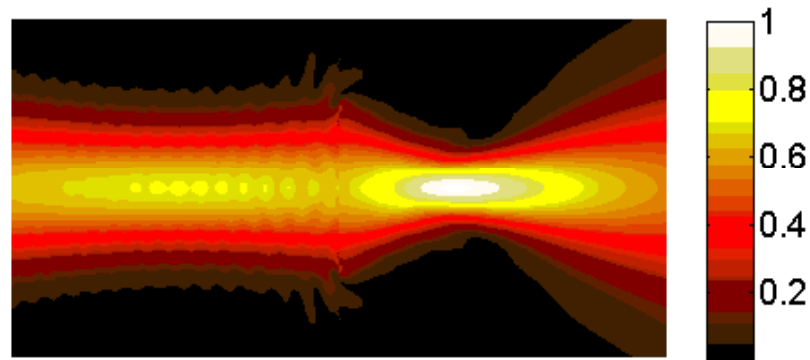


$$\text{Efficiency} = \frac{\text{Metasurface Output Power}}{\text{Metasurface Input Power}}$$

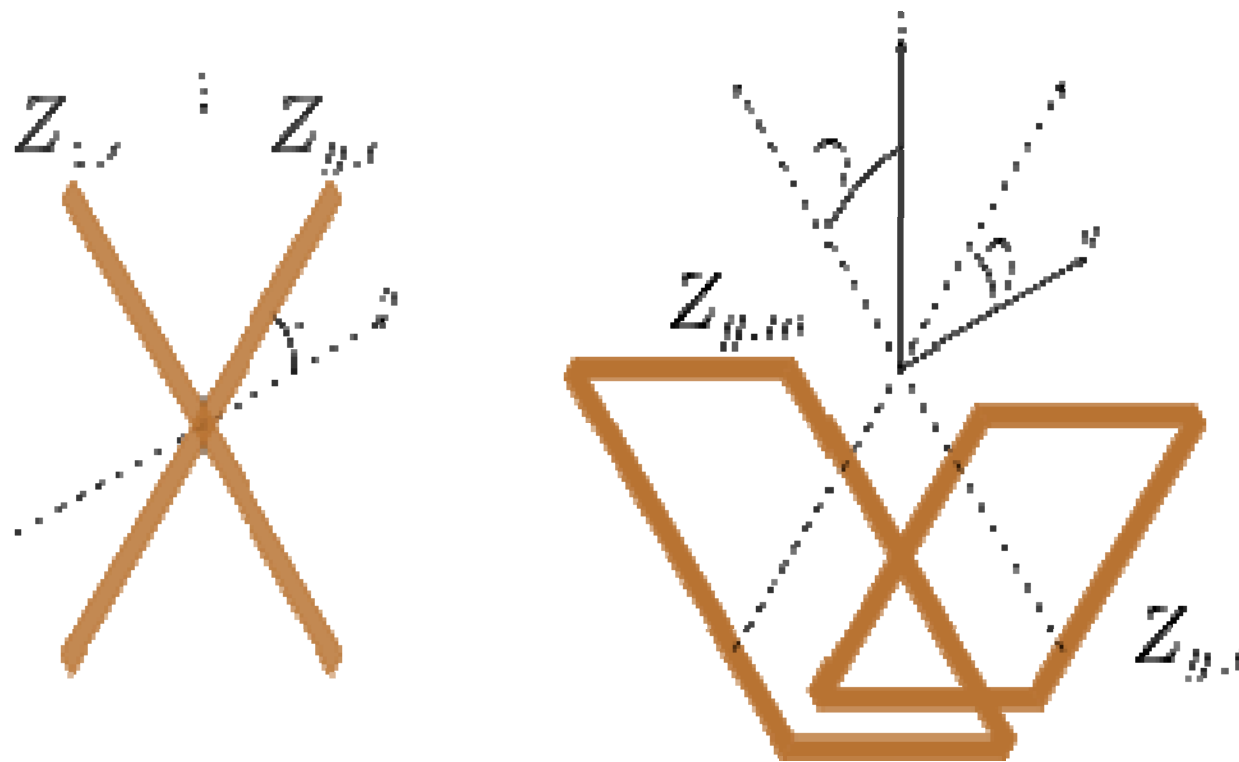
2D Focusing



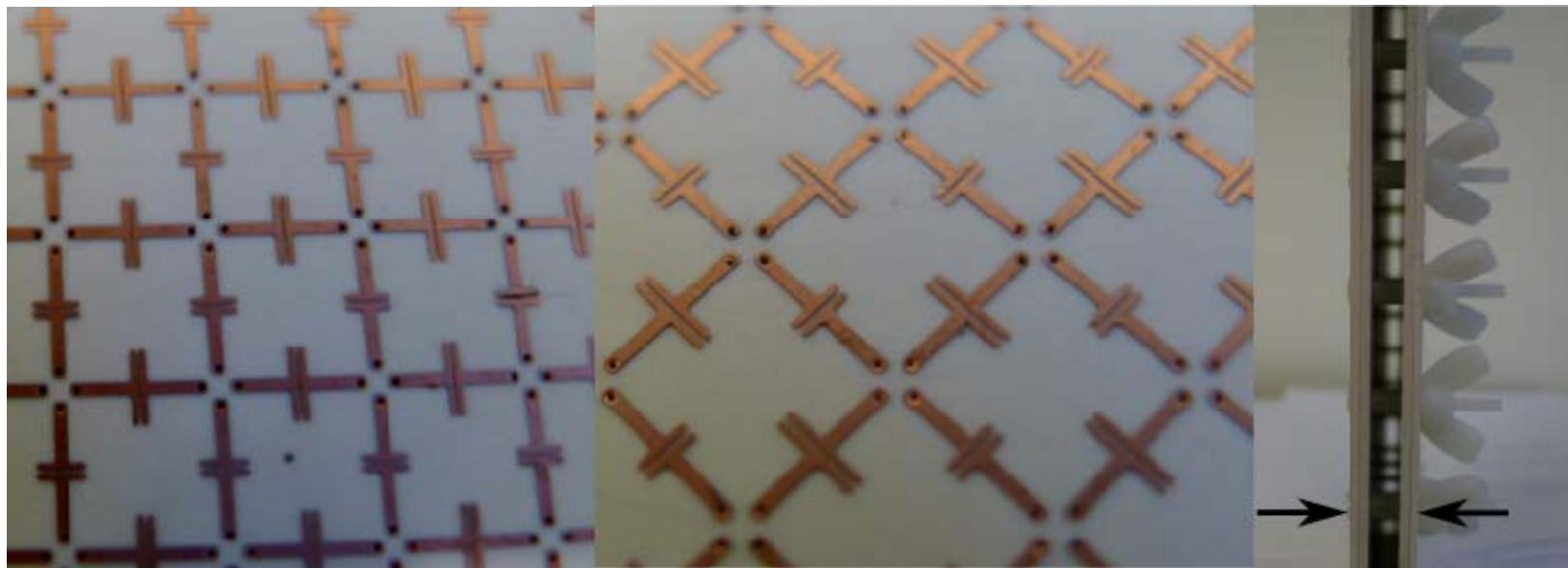
Gaussian-Beam Focusing



TENSOR HUYGENS' METASURFACES



A 90-degree Polarization Rotator



Layer 1

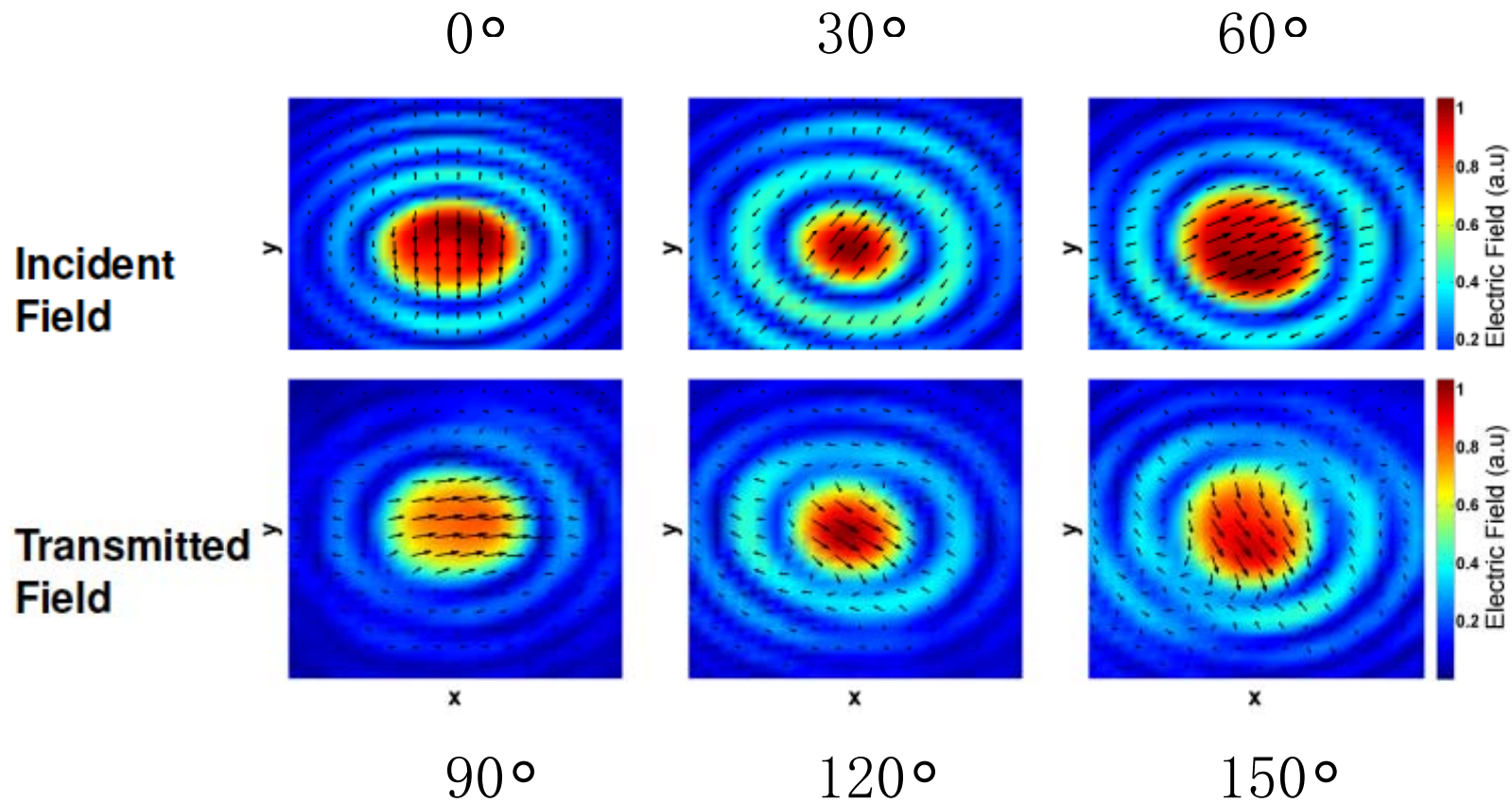
Layer 2

$\lambda/3$

Cascaded and rotated metasurfaces create a bianisotropic effect

Y. Zhao, M. Belkin, and A. Al`u, "Twisted optical metamaterials for planarized ultrathin broadband circular polarizers," *Nature Communications*, vol. 3, p. 870, 2012.

Measurement

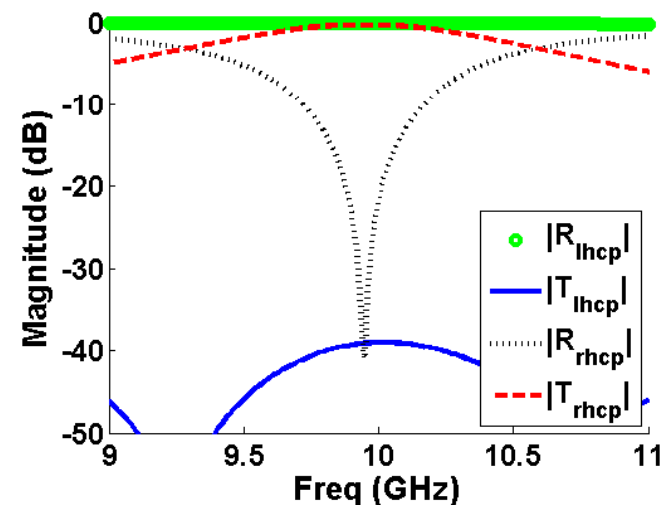
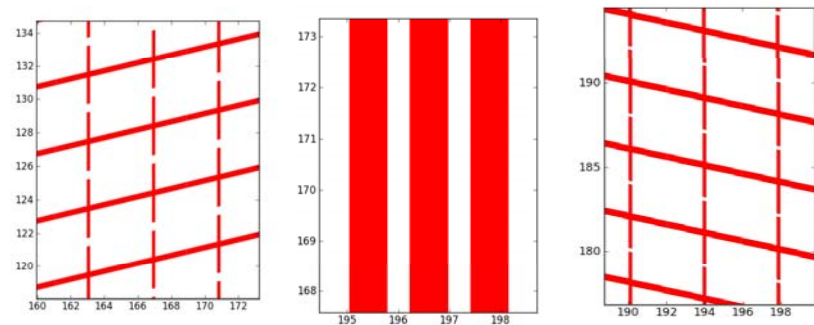


Circular Polarization Selective Surface (CPSS)

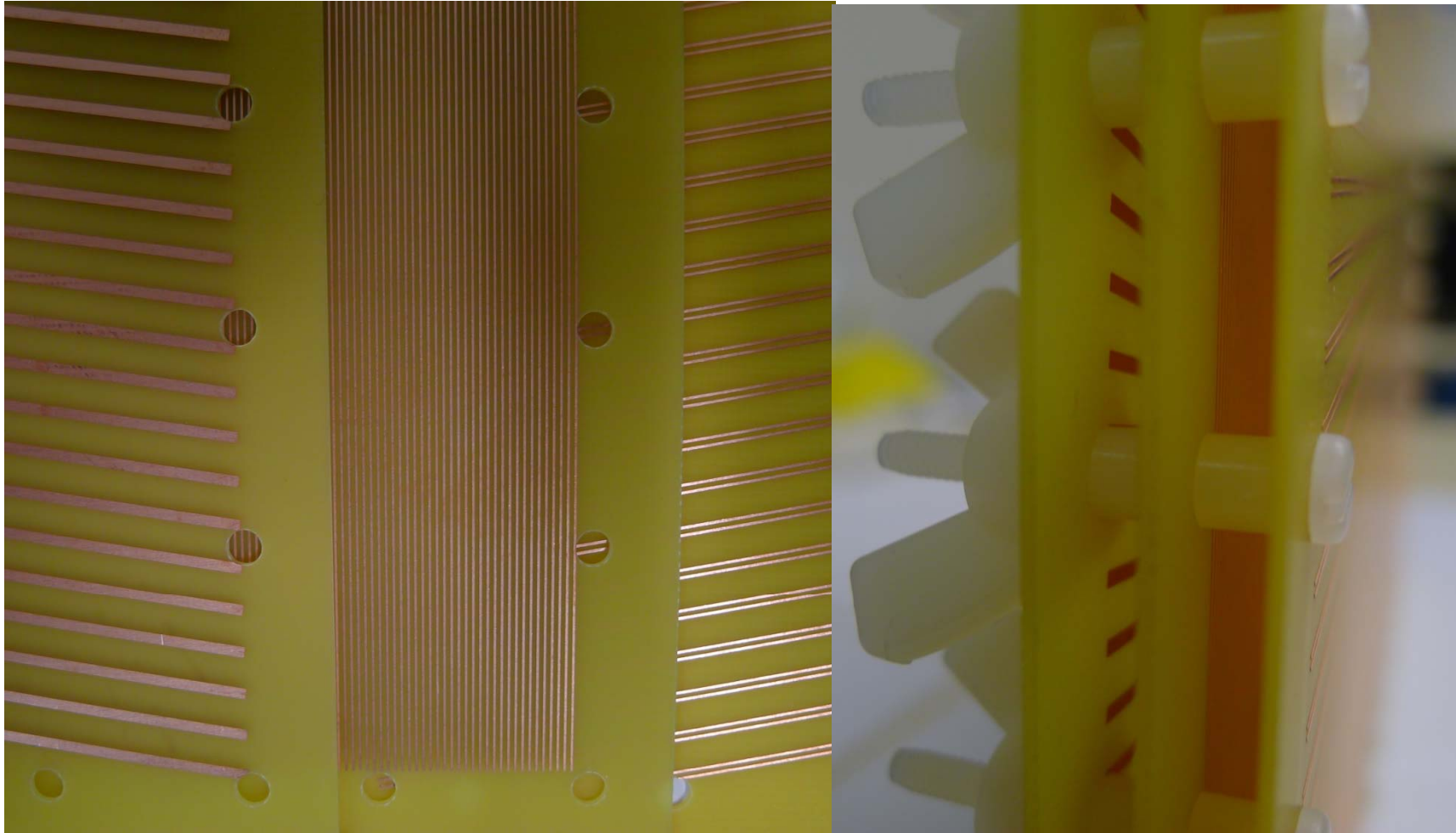
For a circular polarization selective surface we need just three layers. Here our surface transmits right-handed CP while reflecting left-handed CP.

The three layers are shown here. The layers sit on a Rogers substrate and are separated by a $\lambda/7$ gap. The total thickness is $< \lambda/2$. Compared to traditional designs, that design required 7-layers and is 1.6λ thick.

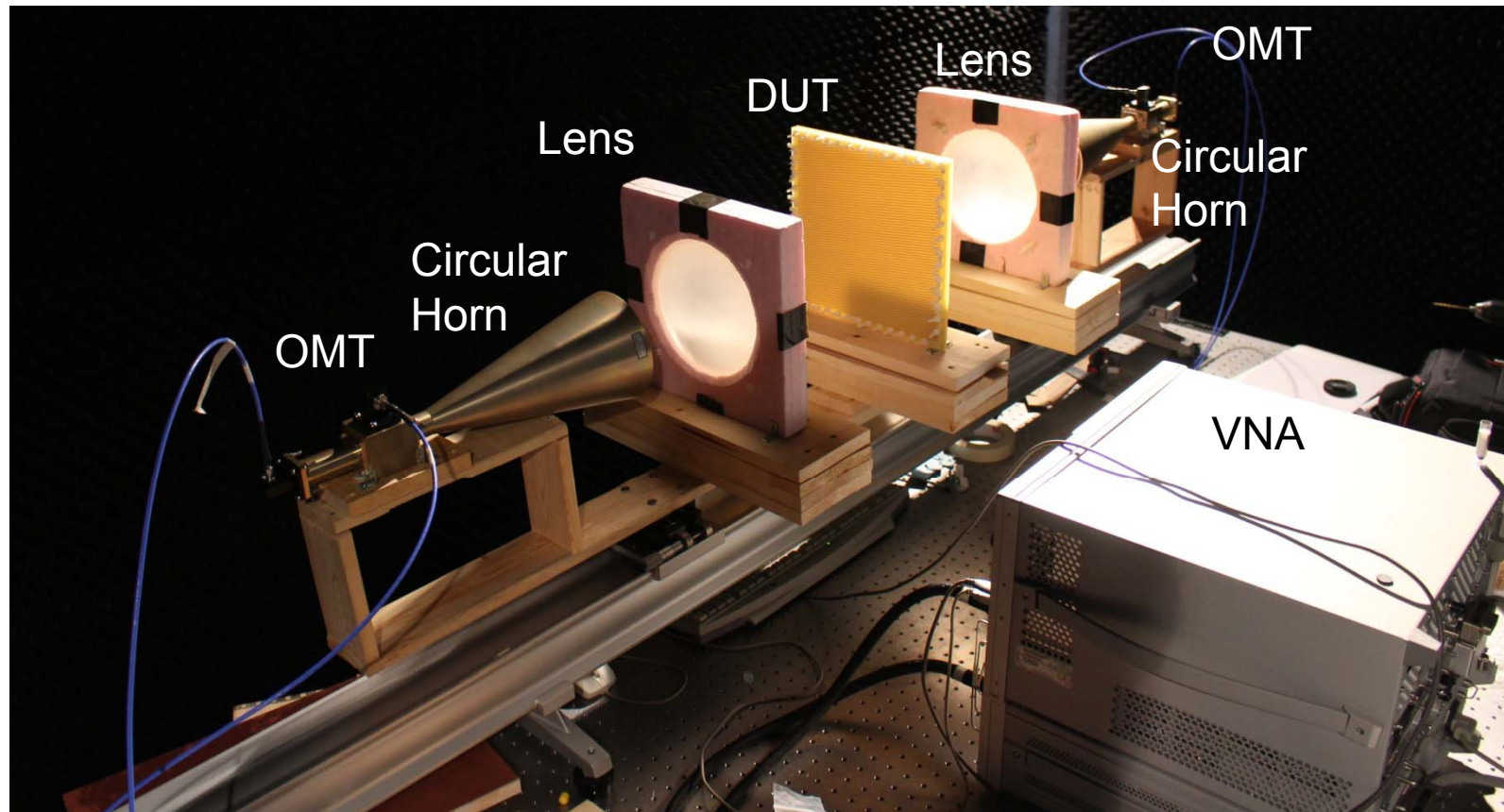
We can see that at 10GHz that right-handed CP is transmitted while left-handed CP is reflected.



Fabricated CPSS

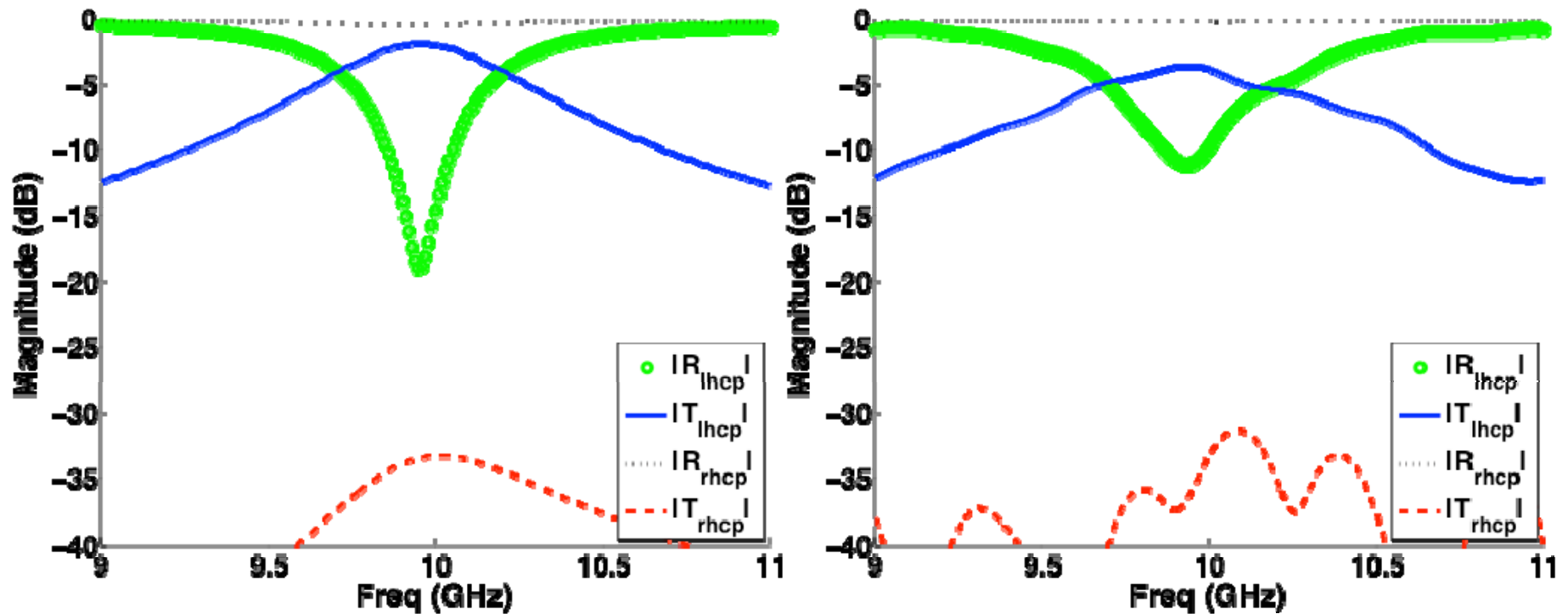


4-Port Quasi-Optical Measurements



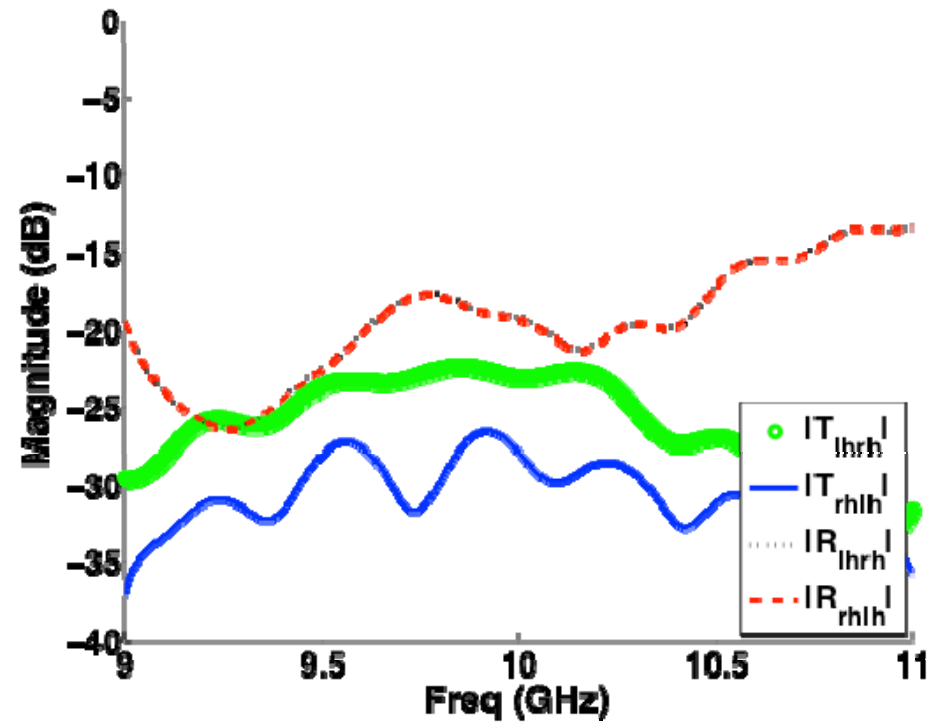
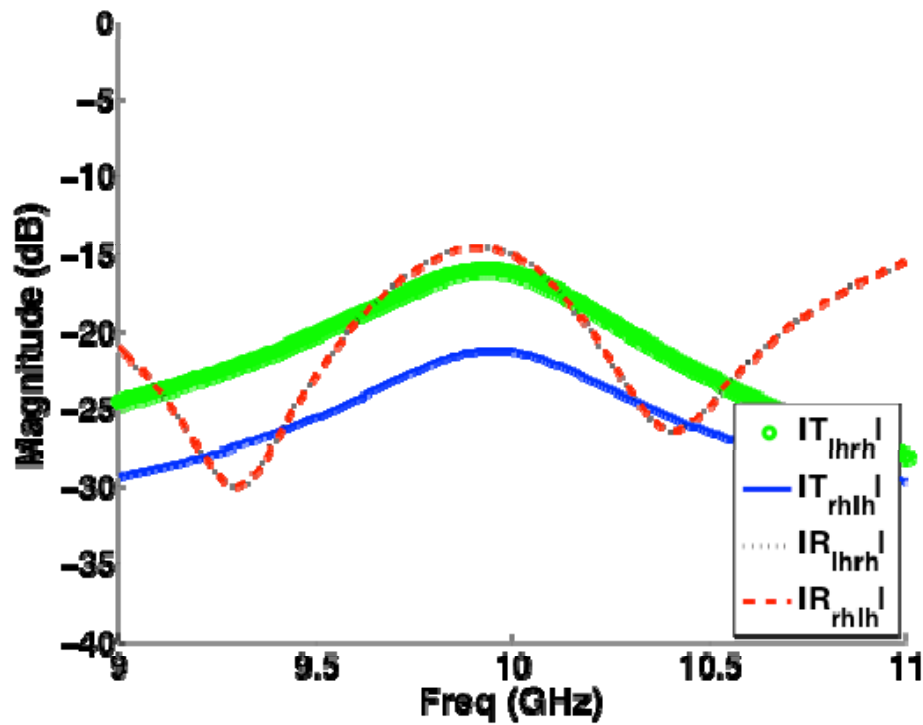
M. Selvanayagam and G.V. Eleftheriades, "Design and measurement of tensor impedance transmitarrays for chiral polarization control", IEEE Trans. on Microwave Theory and Techn., vol. 64, pp. 414-428, Feb. 2016.

Measured Results

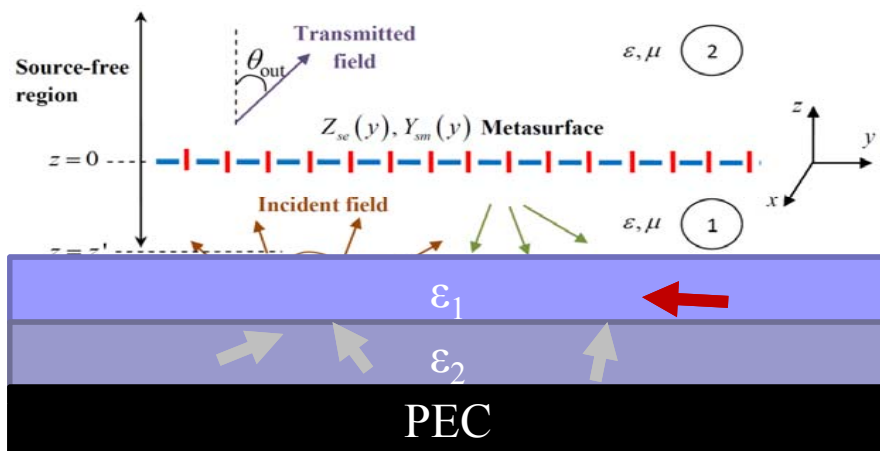


Left-handed CP passes/Right-handed CP is reflected

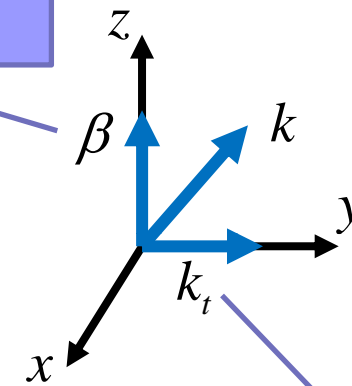
Measured Results



Arbitrary sources to directive radiation

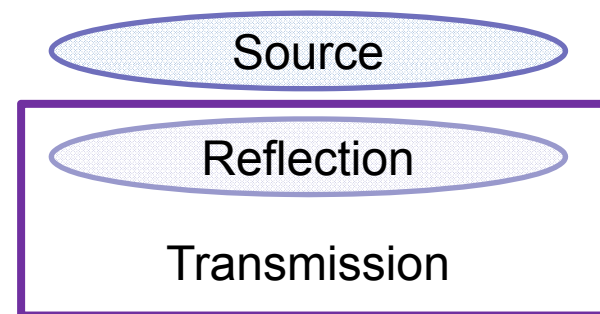


Longitudinal wavenumber



Transverse wavenumber

$$\left\{ \begin{aligned} E_x^{\text{inc}}(y, z) &= k\eta \frac{I_0}{2\pi} \int_{-\infty}^{\infty} \frac{dk_t}{2\beta} f(k_t) e^{-j\beta z} e^{jk_t y} \\ E_x^{\text{ref}}(y, z) &= -k\eta \frac{I_0}{2\pi} \int_{-\infty}^{\infty} \frac{dk_t}{2\beta} \Gamma(k_t) f(k_t) e^{j\beta z} e^{jk_t y} \\ E_x^{\text{trans}}(y, z) &= k\eta \frac{I_0}{2\pi} \int_{-\infty}^{\infty} \frac{dk_t}{2\beta} T(k_t) e^{-j\beta z} e^{jk_t y} \end{aligned} \right.$$



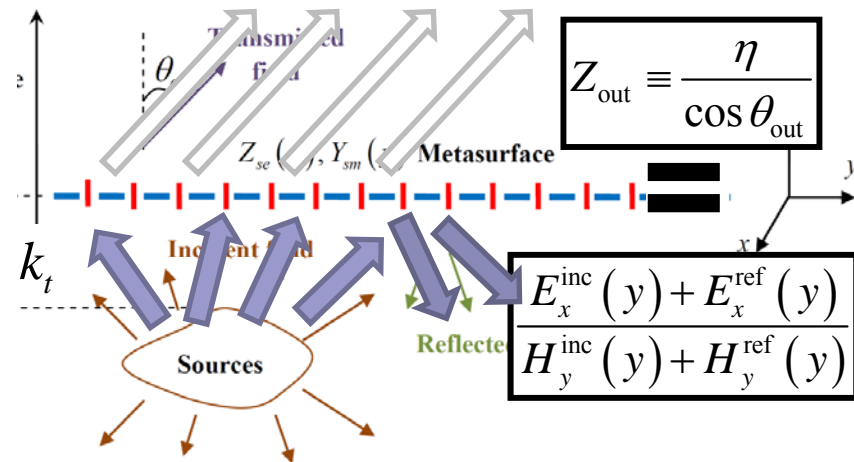
Degrees of Freedom

Passive and Lossless Design

- **Local** impedance equalization

⇒ Reflection

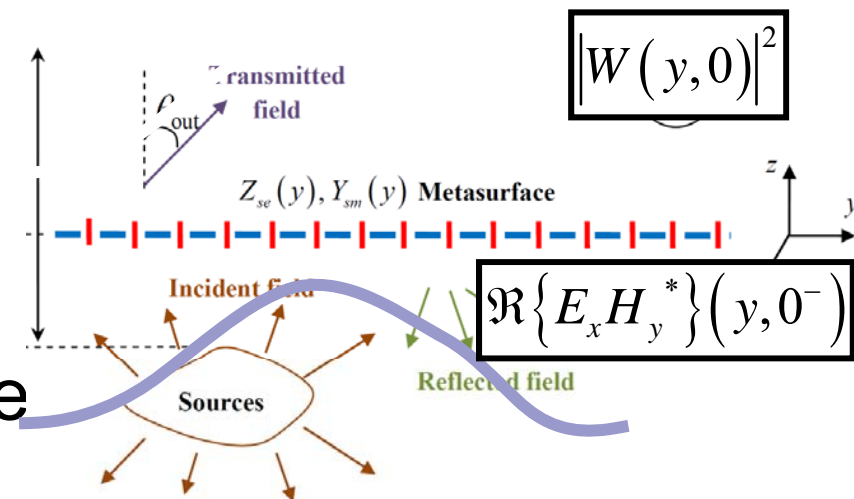
$$\text{Fresnel: } \Gamma(k_t) = \frac{k \cos \theta_{\text{out}} - \beta}{k \cos \theta_{\text{out}} + \beta}$$



- **Local** power conservation

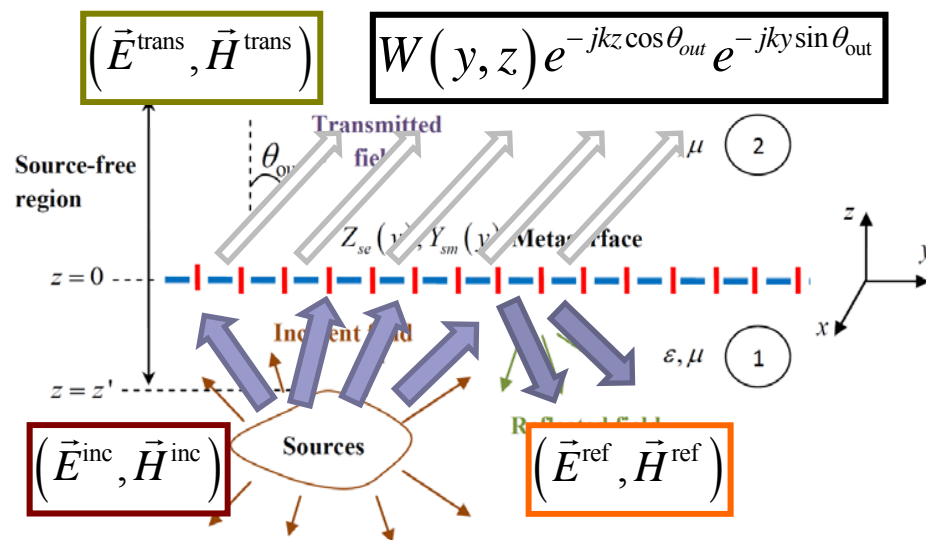
⇒ Transmission

⇒ Aperture follows incident power profile



Huygens' Metasurface (HMS) Design

- Source, reflection, transmission stipulated



$$\varphi(y, 0^+) = ky \sin \theta_{out}$$

$$\varphi(y, 0^-) = \angle \{ E_x^{inc}(y, 0^-) + E_x^{ref}(y, 0^-) \}$$

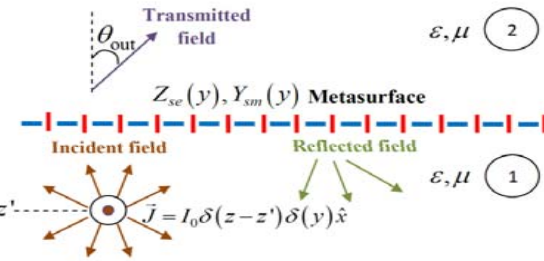
Magnitude Phase

$$Y_{sm}(y) = -j \frac{\cos \theta_{out}}{2\eta} \cot \left(\frac{\varphi(y, 0^+) - \varphi(y, 0^-)}{2} \right)$$

$$Z_{se}(y) = -j \frac{\eta}{2 \cos \theta_{out}} \cot \left(\frac{\varphi(y, 0^+) - \varphi(y, 0^-)}{2} \right)$$

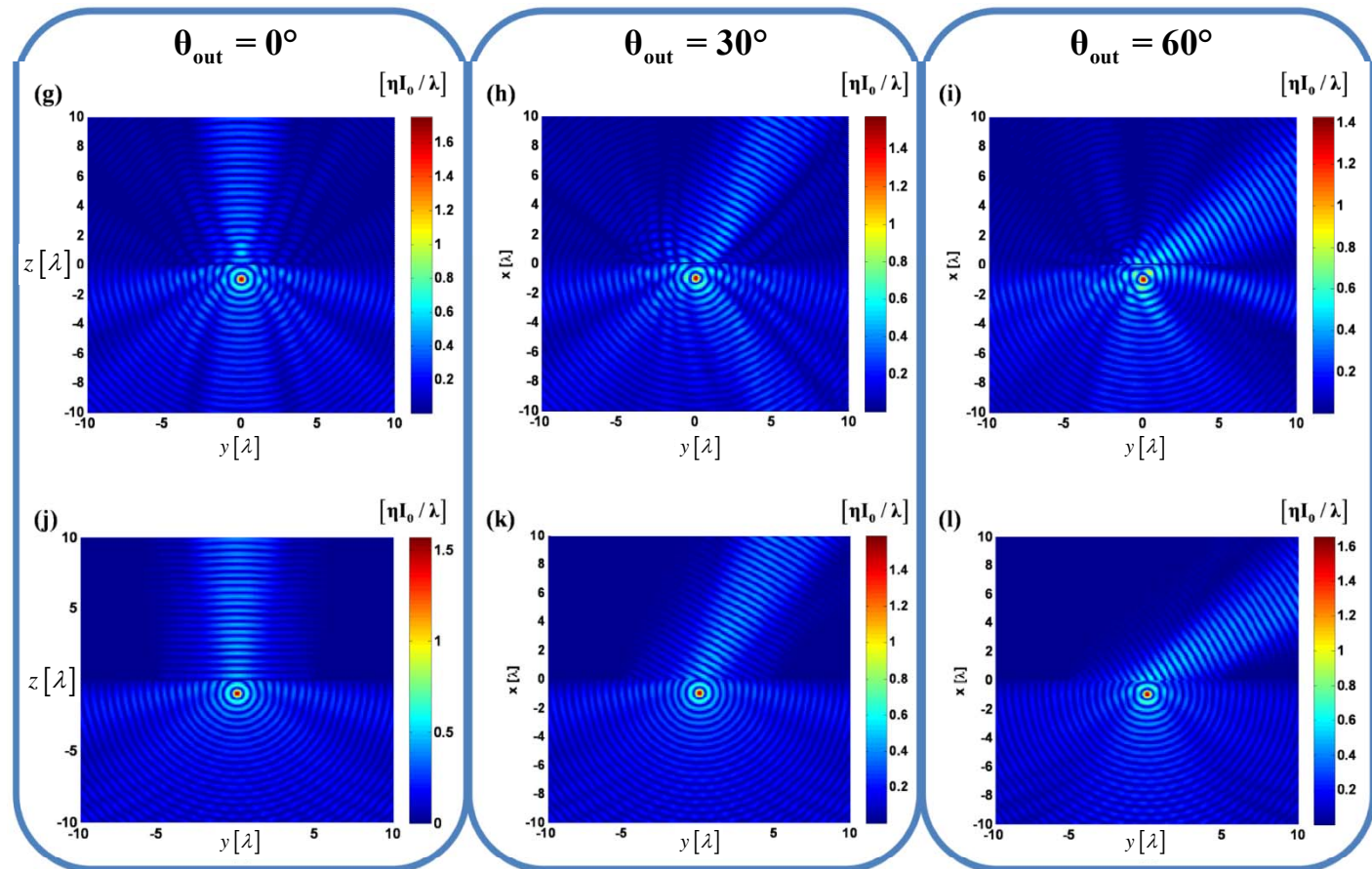


Electric Line Source

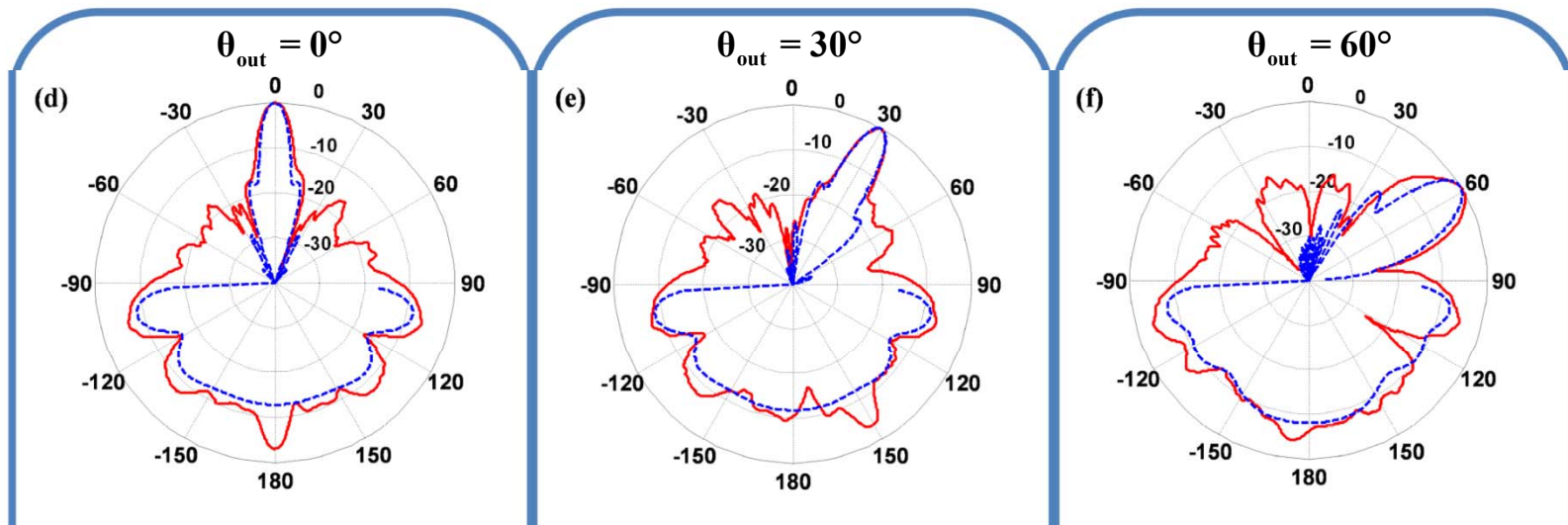
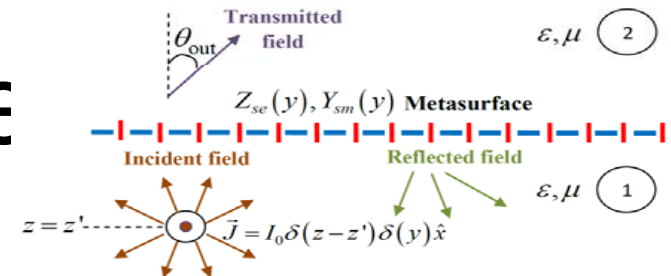


Finite-element simulation
("Implementation")

Semi-analytical theory
(Design)



Electric Line Source

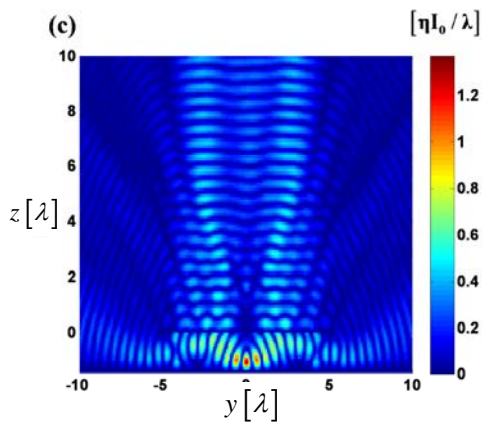


Finite-element simulation
("Implementation")

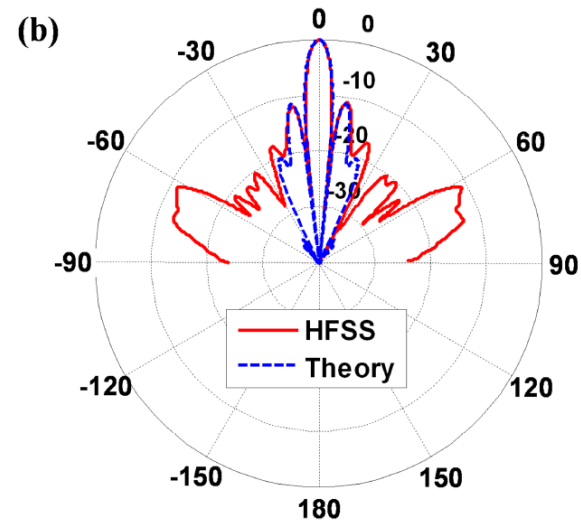
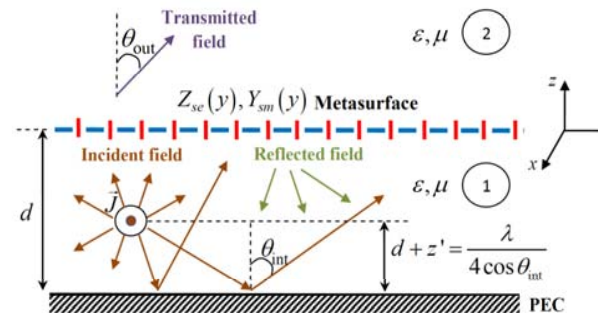
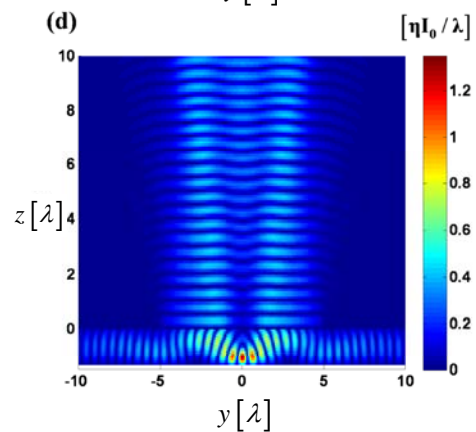
Semi-analytical theory
(Design)

Electric Line Source and PEC

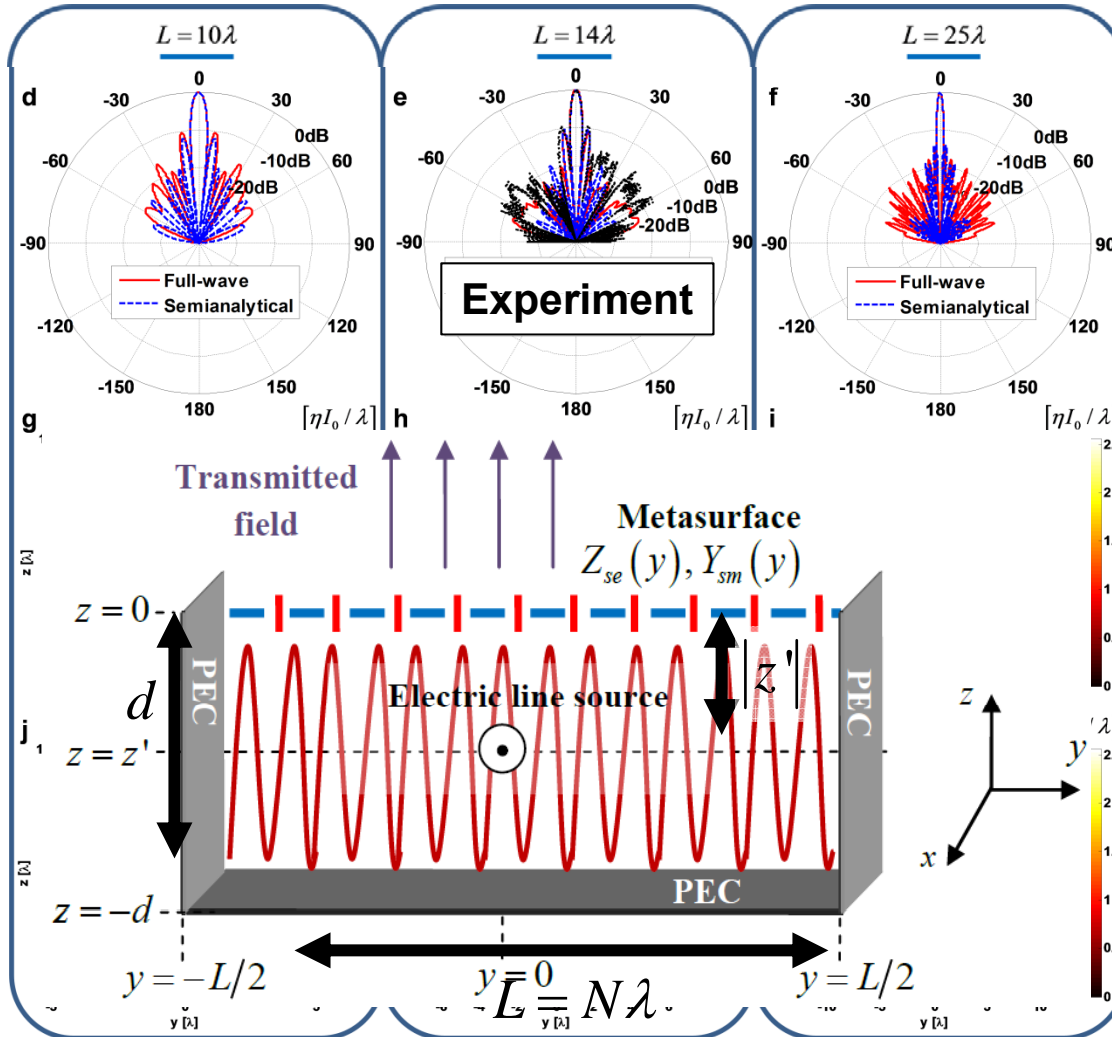
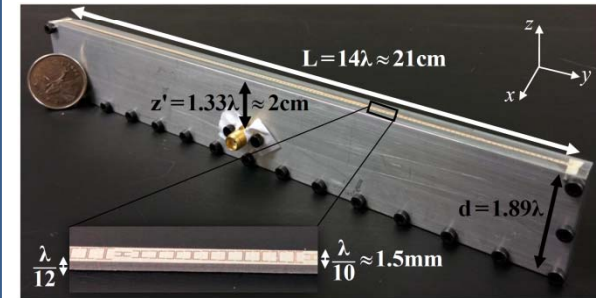
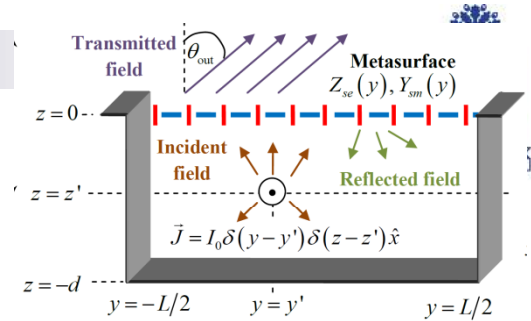
Finite
elements
simulation



Semi-
analytical
theory

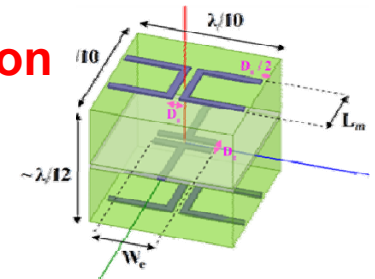


Cavity-excited HMS antenna *(solves the aperture efficiency vs radiation efficiency tradeoff in leaky-wave antennas)*



$f = 20\text{GHz}$

Full-wave
(Discretization, losses)



Semianalytical

Control of Radiation Pattern

Reduced side-lobe level

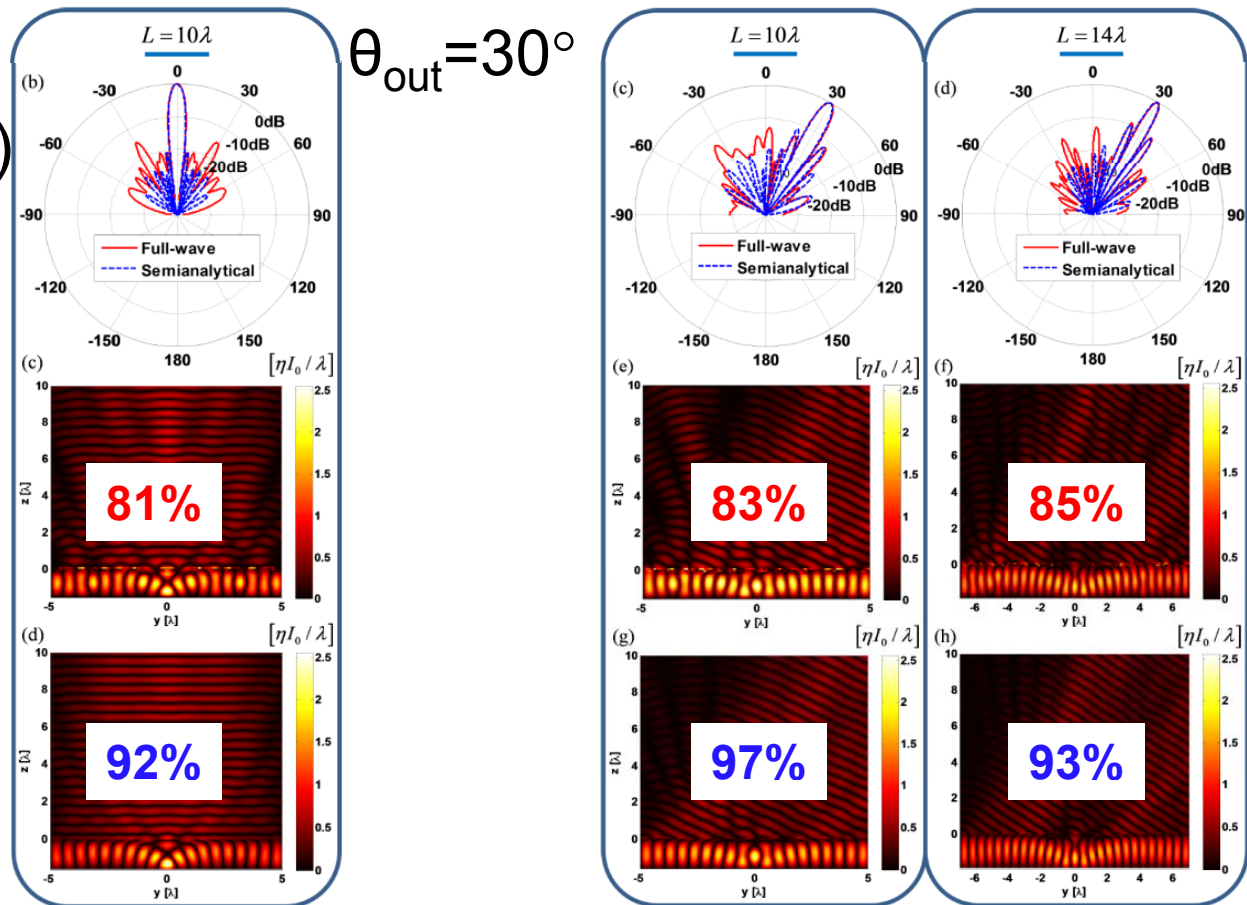
- SLL = -20dB
(10dB reduction)

Full-wave
(Discretization,
losses)

Semianalytical

Direction of main beam

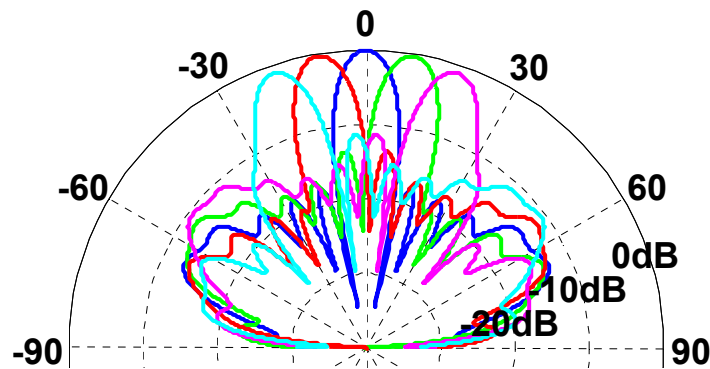
$$\theta_{\text{out}} = 30^\circ$$



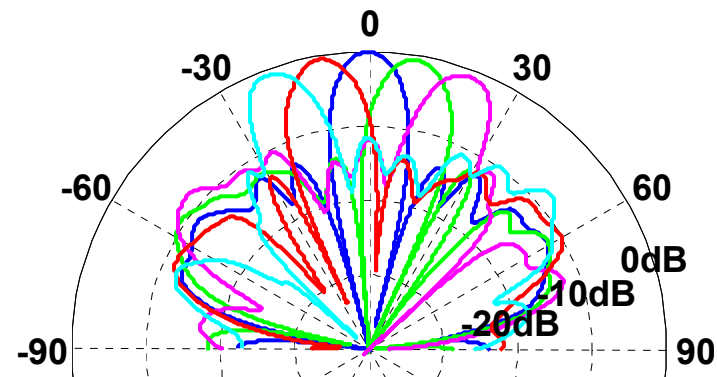
Switched-beam Antenna

| Shift | Main beam | | 3dB Beamwidth | | Directivity [dBi] | | Aperture efficiency | |
|---------------------------|--------------------|--------------------|---------------|--------------|-------------------|------|---------------------|------|
| | Theory | HFSS | Theory | HFSS | Theory | HFSS | Theory | HFSS |
| $\Delta y=0$ | 0° | 0° | 10.1° | 12.1° | 14.3 | 13.2 | 86% | 67% |
| $\Delta y=\pm 0.6\lambda$ | $\cdot 9.5^\circ$ | $\cdot 9.8^\circ$ | 10.2° | 12.7° | 14.1 | 12.7 | 83% | 60% |
| $\Delta y=\pm 1.2\lambda$ | $\cdot 18.7^\circ$ | $\cdot 20.5^\circ$ | 10.7° | 12.7° | 13.3 | 12.4 | 72% | 59% |

Semianalytical



Full-wave





Reflectionless Wide-Angle Refracting Metasurfaces

Joseph P. S. Wong, *Student Member, IEEE*, Ariel Epstein, *Member, IEEE*, and George V. Eleftheriades, *Fellow, IEEE*

Abstract—We hereby report a solution to the problem of reflections from passive lossless refracting metasurfaces that works even at wide deflection angles. The phenomenon of reflections is due to not accounting for the local wave-impedance mismatch at the source and load faces of the metasurface; this cannot be fully mitigated even with an impedance-equalized Huygens' (IEH) metasurface. The solution is demonstrated to be enabled through the correct application of generalized, instead of canonical, scattering parameters. The canonical and IEH approaches are compared to the generalized scattering parameter approach. It is seen that though the approaches are similar at low-to-moderate levels of refraction, at wide-angle refraction only the generalized S-matrix approach is capable of good matching. This is demonstrated via full-wave simulations, for refraction from normal incidence, using an asymmetric structure comprising three cascaded admittance surfaces.

Index Terms—Matching, metasurfaces, refraction, scattering parameters, wide-angle.

I. INTRODUCTION

VARIOUS perspectives exist in the design of metasurfaces. These include frequency selective surfaces [1], impedance surfaces [2], as well as Huygens' metasurfaces [3], [4], among others. Their embodiments are low-profile, and they can achieve remarkable wave-manipulation capabilities [5]. In addition, Huygens' metasurfaces show good matching and insertion loss [6]. On the micro level, one factor common to all these approaches is the synthesis of unit cells in an infinite homogeneous array using microwave network theory. Subsequently, in the finite inhomogeneous embodiments (e.g., for refraction and focusing), the changes along the aperture are assumed to be slowly varying, and the micro-level unit cell results remain valid due to the "local periodicity" [7].

On this macro level of the finite inhomogeneous metasurface, there exist two common design approaches. In terms of the canonical scattering parameters $[S]$, one can enforce $S_{11}(x) = S_{22}(x) = 0$ to attempt to eliminate reflections, and $S_{21}(x) = S_{12}(x) = e^{j\phi(x)}$ to provide a phase shift $\phi(x)$ over the aperture position x . This we term the canonical approach [7], [8]. Alternatively, using Schelkunoff's equivalence principle, one can stipulate the tangential electromagnetic fields over the aperture position. Then, effective boundary conditions determine the required surface polarizabilities to

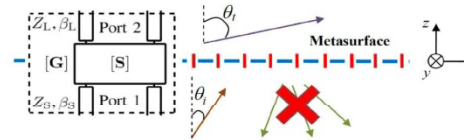


Fig. 1. Illustration of a metasurface refracting a plane wave from θ_i to θ_t , without reflections. This is described using the generalized S-parameters $[G]$.

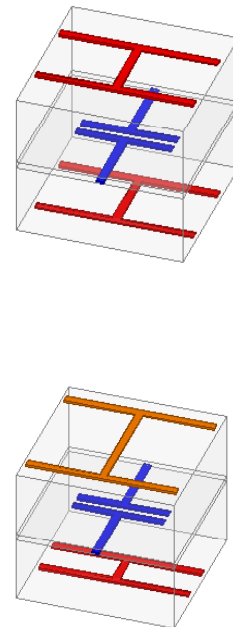
support these fields [9], which can be expressed as surface impedances and admittances [3], [4]. In [10], the correspondence between Schelkunoff's equivalence principle and circuit concepts is demonstrated, relating these surface impedances and admittances to microwave network theory. This we term the Huygens' approach.

In [3], reflectionless plane-wave refraction is investigated using the equivalence principle. However, this is found to require complex impedances and admittances, resulting in Huygens' sources that are not passive and lossless. Numerical optimization is used to fit the results to a purely reactive solution. In [4] and [11], slight reflections are permitted to avoid active or lossy Huygens' sources, permitting a rigorous analytical formulation. This approach, which we term the impedance-equalized Huygens' (IEH) approach, is implemented in [6] using [10]. The experimental results in these cases are similar to the ones corresponding to the canonical approach [8]: As long as the refraction angles are moderate, the matching is good.

In this letter, we show that wide angles of refraction produce a dramatic increase in reflection using these existing approaches. This phenomenon is inherent to $[S]$ because of the identical incident and refracted wave impedances assumed there, when in fact there is a mismatch. The correct description of reflectionless plane-wave refraction is thus afforded by the use of generalized scattering parameters $[G]$. Note that $[G]$ exists for both pseudo [12] and power waves [13], but these in general are not equivalent and cannot be applied in the same contexts [14]. In their application to positive but dissimilar wave impedances considered here, these are equivalent, and matching becomes near-perfect even in the case of wide-angle plane-wave refraction.

II. MACRO- AND MICRO-LEVEL DESCRIPTIONS OF REFLECTIONLESS PLANE-WAVE REFRACTION

Fig. 1 illustrates a metasurface refracting a plane wave from θ_i to θ_t without reflections. On the macro level, this phenomenon is correctly described in terms of a reciprocal $[G]$, where



Manuscript received October 19, 2015; accepted December 01, 2015. Date of publication December 04, 2015; date of current version April 13, 2016.

The authors are with the Department of Electrical and Computer Engineering, University of Toronto, Toronto, ON M5S 3G4, Canada (e-mail: gelefth@ece.utoronto.ca).

Color versions of one or more of the figures in this letter are available online at <http://ieeexplore.ieee.org>.

Digital Object Identifier 10.1109/LAWP.2015.2505629

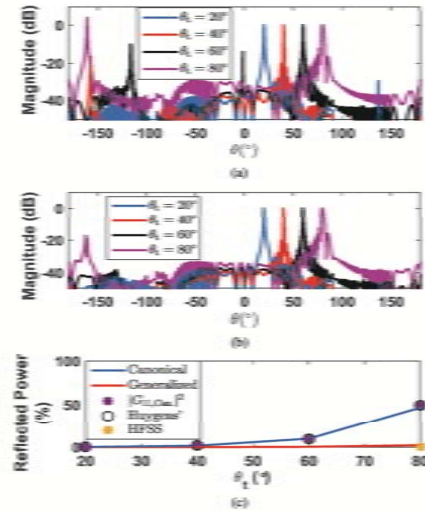


Fig. 3. Radiation patterns for $\theta_i = 0^\circ$, and θ_r from 20° to 80° using the different approaches. (a) Canonical, (b) generalized, and (c) the reflected power percentages.

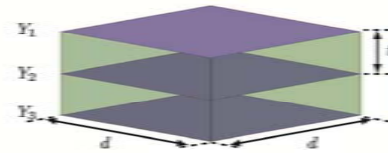


Fig. 4. Topology used to implement $[\mathbf{G}]$, corresponding to a reciprocal but physically asymmetric structure.

symmetric structure. However, in the generalized approach, this transformation yields $S_{11}(x) \neq S_{22}(x)$, which corresponds to a physically asymmetric structure. In addition, because of reciprocity, it is recognized that there are three unknowns in $[\mathbf{G}]$, therefore the solution requires 3 degrees of freedom. Thus, the following topology can be used as shown in Fig. 4. It consists of three different admittance sheets. This is similar to [8], except that all the admittance sheets here are independent.

Here, t is the substrate thickness, and d the transverse dimensions of the unit cell. The admittance of each sheet is denoted as Y_1 , Y_2 , and Y_3 , respectively. From network theory, the $ABCD$ -parameters of the constituent admittance sheets and substrates can be respectively expressed as [13]

$$[\mathbf{M}_{\text{TL}}] = \begin{bmatrix} \cos(\beta_0 t) & jZ_0 \sin(\beta_0 t) \\ j\frac{1}{Z_0} \sin(\beta_0 t) & \cos(\beta_0 t) \end{bmatrix} \quad (4)$$

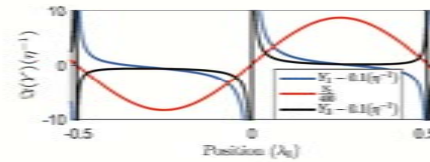


Fig. 5. One period of Y_1 , Y_2 , and Y_3 , with their values scaled and offset for better comparison of the modulation.

and

$$[\mathbf{M}_Y] = \begin{bmatrix} 1 & 0 \\ Y & 1 \end{bmatrix}. \quad (5)$$

Here, β_0 is the propagation constant in the lossless substrate, and Z_0 its characteristic impedance. The $ABCD$ parameters of the entire unit cell in Fig. 4 comprising all the admittance sheets are given as

$$[\mathbf{M}] = [\mathbf{M}_{Y,1}][\mathbf{M}_{\text{TL}}][\mathbf{M}_{Y,2}][\mathbf{M}_{\text{TL}}][\mathbf{M}_{Y,3}] \quad (6)$$

The system in (6) can be solved analytically for Y_1 , Y_2 , and Y_3 as follows:

$$Y_1 = \frac{j \det[\mathbf{Z}] \cos(\beta_0 t) + Z_0(Z_{22} + Z_{12}) \sin(\beta_0 t)}{Z_0 \det[\mathbf{Z}] \sin(\beta_0 t)} \quad (7)$$

$$Y_2 = \frac{2 \det[\mathbf{Z}] - j Z_0 Z_{12} \sin(2\beta_0 t)}{Z_0^2 Z_{12} (\cos(2\beta_0 t) - 1)} \quad (8)$$

$$Y_3 = \frac{j \det[\mathbf{Z}] \cos(\beta_0 t) + Z_0(Z_{11} + Z_{12}) \sin(\beta_0 t)}{Z_0 \det[\mathbf{Z}] \sin(\beta_0 t)} \quad (9)$$

where $\det[\mathbf{Z}] = Z_{11}Z_{22} - Z_{12}^2$ is the determinant of $[\mathbf{Z}]$ whose components correspond to (3), and $[\mathbf{M}]$ can be transformed from $[\mathbf{Z}]$, e.g., using [13]. This procedure for unit cell design has been verified in HFSS using cascaded sheets enforcing the suitable impedance boundary conditions.

V. FULL-WAVE DEMONSTRATION OF WIDE-ANGLE REFRACTING METASURFACE FOLLOWING $[\mathbf{G}]$

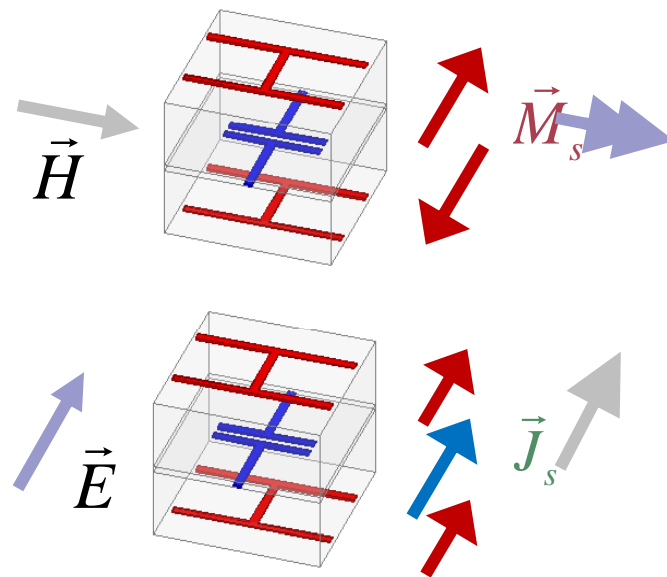
Here, using the unit cell topology in Fig. 4, a metasurface for $\theta_i = 0^\circ$ to $\theta_r = 80^\circ$ TE-polarized refraction is implemented in HFSS; the admittance sheets are realized again using impedance boundary conditions. The substrate and geometrical parameters are chosen to be $d = \lambda_0/17.74$, $t = 5$ mil, $\epsilon_R = 10.2$, $\tan \delta = 0$, and $f_0 = 10.0$ GHz. These substrate values correspond to RT/duroid 6010 of commercially available thickness, but neglecting losses. The chosen discretization of $d = \lambda_0/17.74$ results in 18 unit cells per period. Fig. 5 presents one period of the Y_1 , Y_2 , and Y_3 admittance values necessary to enforce reflectionless $\theta_i = 0^\circ$ to $\theta_r = 80^\circ$ plane-wave refraction. The truncation of extreme values in impedance profiles is investigated in [15] and shown to have only a mild impact on IEH efficiency.

The simulation domain is $4\lambda_0$ by $18d$ and consists of one period of unit cells contained within master and slave boundaries, with Floquet ports at either end. The only Floquet modes of interest are the propagating ones, which in this case are the

Ω -Bianisotropic Metasurfaces

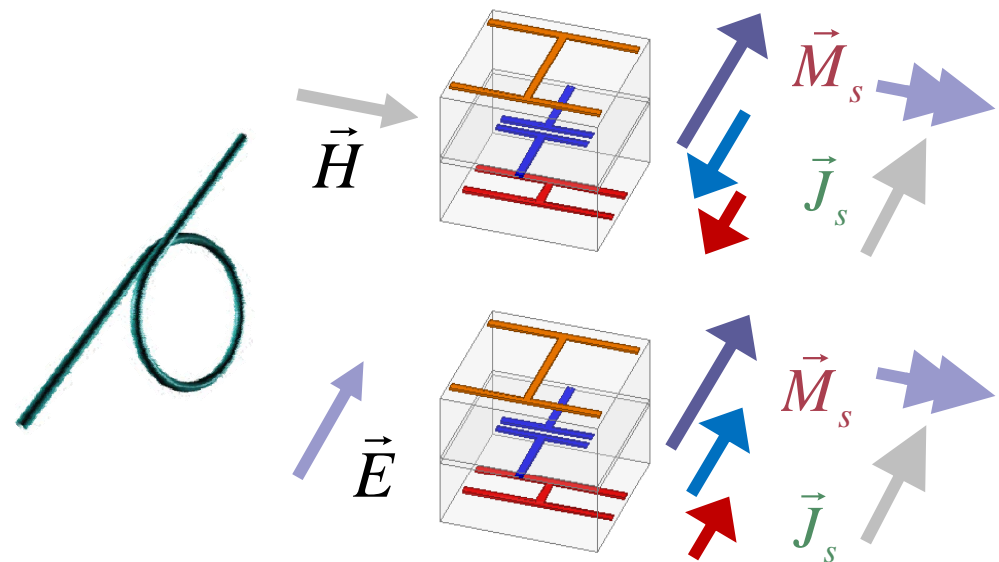
Huygens' metasurfaces

- **Electric** impedance
- **Magnetic** admittance



Ω -Bianisotropic metasurfaces

- **Electric** impedance
- **Magnetic** admittance
- **Magnetolectric coupling**

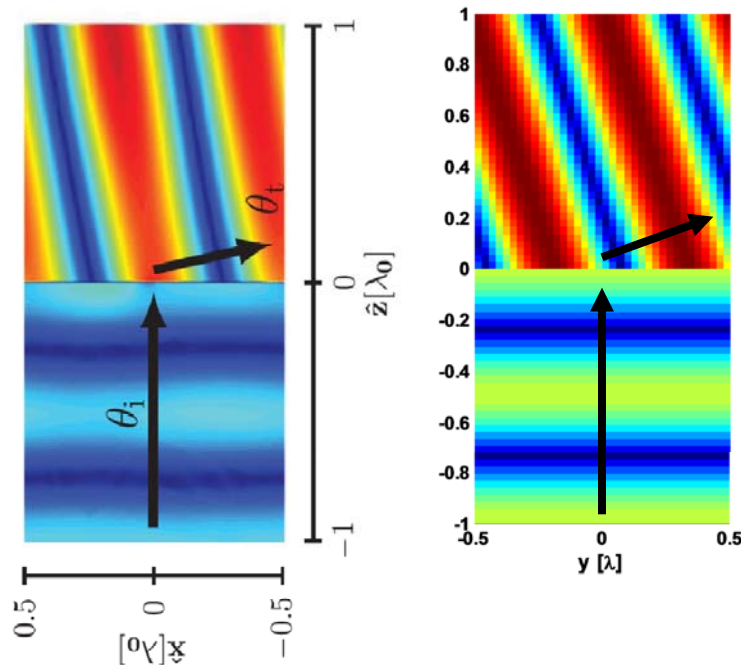


Y. Ra'di, V. Asadchy and S. A. Tretyakov, *IEEE Trans. Antennas Propag.*, **62**, 7 (2014)

J. Wong, A. Epstein, and GV Eleftheriades, *IEEE Antennas Wireless Propag. Lett.*, vol 15, (2016).

Extreme Angle Refraction

Refraction



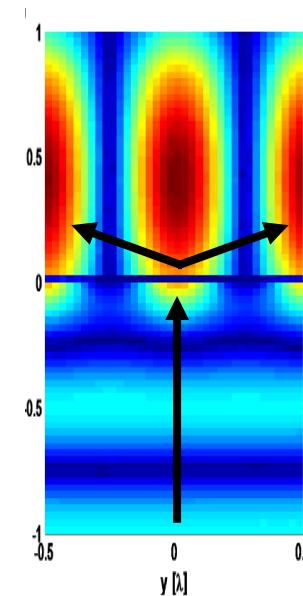
$0^\circ \rightarrow 80^\circ$
Efficiency:
98.9%

(Huygens': 50%)

$0^\circ \rightarrow 72^\circ$
Efficiency:
99.5%

(Huygens': 73%)

Beam splitter



$0^\circ \rightarrow \pm 72^\circ$
Efficiency: 98% (1:1)

* J. Wong, A. Epstein, and GV Eleftheriades, *IEEE Antennas Wireless Propag. Lett.*, (2016).

* Epstein and Eleftheriades, **accepted** to *APS/URSI Puerto Rico* (2016).

Floquet-Bloch (FB) analysis (arbitrary angle of incidence)

■ Refracting HMS $\theta_{in} \rightarrow \theta_{out}$

$$\frac{Z_{se}(y)}{Z_{out}} = \frac{Y_{sm}(y)}{Y_{out}} = -j \frac{1}{2} \cot \left[\frac{ky(\sin \theta_{out} - \sin \theta_{in})}{2} \right]$$

■ Designated excitation

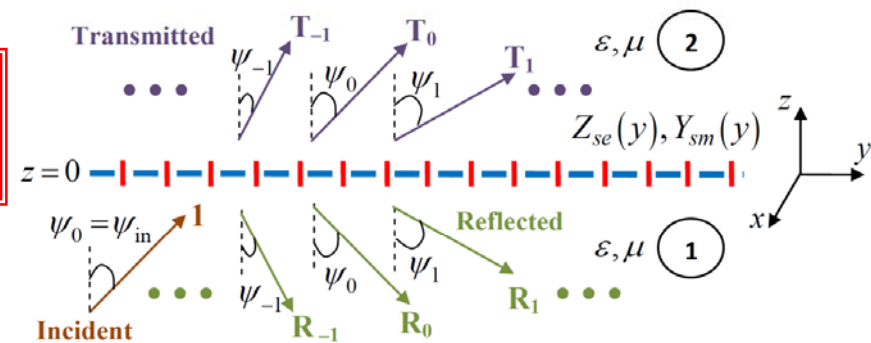
- **Only two FB modes:** specular reflection and desirable refraction (the rest vanish, **unlike grating**)

$$\psi_{in} = \theta_{in}$$

■ Arbitrary ray excitations

- **Refraction (n=1) is dominant** over scattering to other directions (**little sensitivity** to angle of incidence)

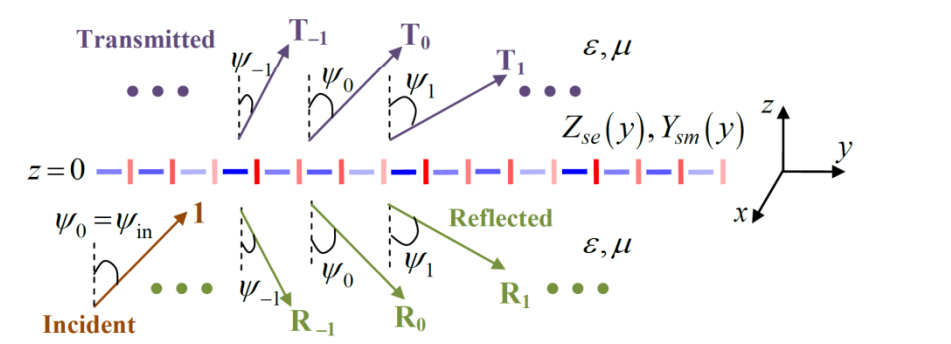
$$\psi_{in} \neq \theta_{in}$$

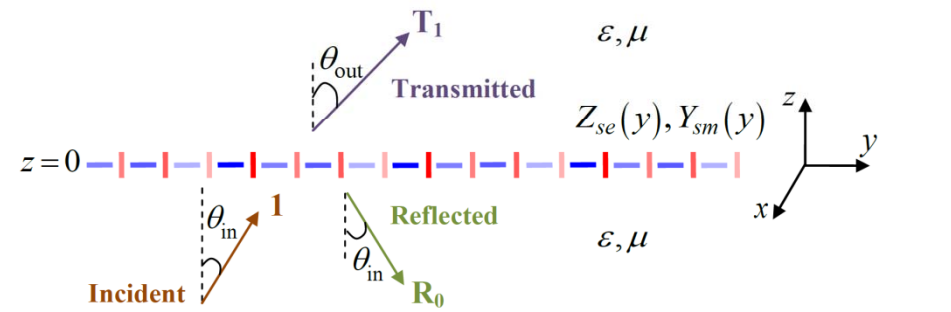


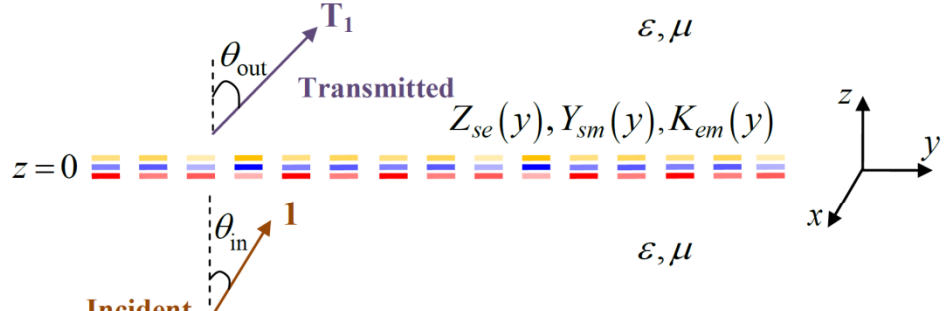
$$\left\{ \begin{aligned} E_x^{inc}(y, z) &= \frac{k\eta I_0}{2} e^{-jkz \cos \psi_{in}} e^{-jk y \sin \psi_{in}} \\ E_x^{ref}(y, z) &= -\frac{k\eta I_0}{2} \sum_{n=-\infty}^{\infty} R_n e^{jkz \cos \psi_n} e^{-jk y \sin \psi_n} \\ E_x^{trans}(y, z) &= \frac{k\eta I_0}{2} \sum_{n=-\infty}^{\infty} T_n e^{-jkz \cos \psi_n} e^{-jk y \sin \psi_n} \end{aligned} \right.$$

Floquet-Bloch Analysis

| Metasurface | Angle of incidence | Refraction Efficiency |
|-------------------------|--------------------------|--|
| Huygens' | Arbitrary ψ_{in} | $\frac{\cos \psi_{out}}{\cos \psi_{in}} 1 - \Gamma_0 ^2 1 + \Gamma_1 ^2$ |
| Huygens' | Designated θ_{in} | $\frac{\cos \theta_{out}}{\cos \theta_{in}} 1 - \Gamma_0 ^2$ |
| Ω -Bianisotropic | Designated θ_{in} | 1 |

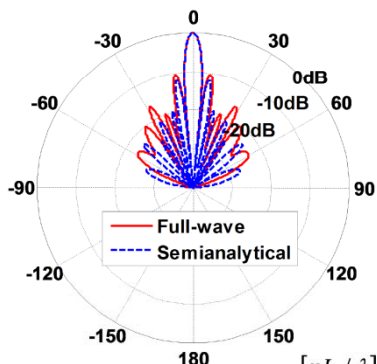
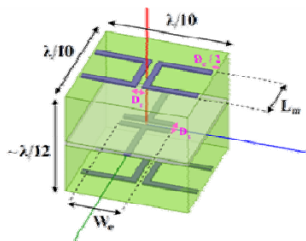




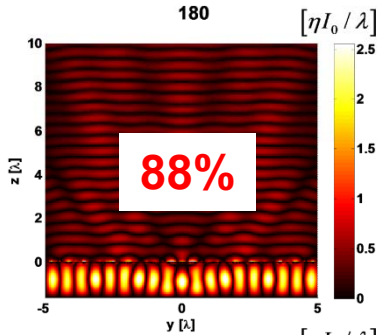


HMS Vs. Ω -BMS

$f = 20\text{GHz}$



**Full-wave
(Discretization,
losses)**

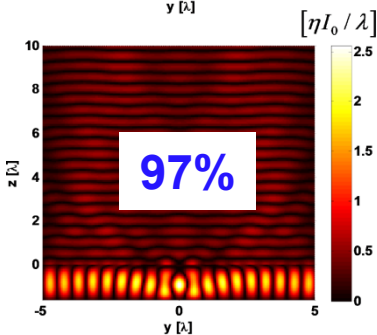


$$\eta_{apt} = \frac{L_{eff}}{L}$$

$$D = 2\pi(L_{eff} / \lambda)$$

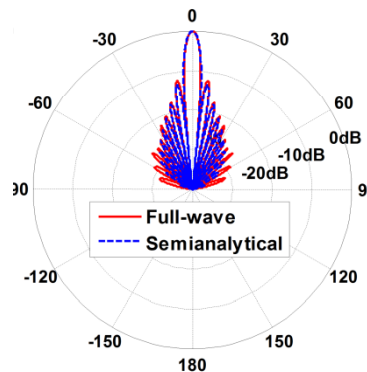
Semianalytical

$$d = 1.61\lambda$$

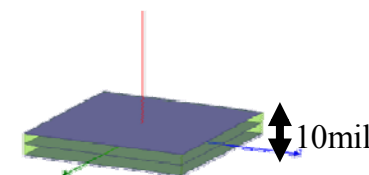


$$L = 10\lambda$$

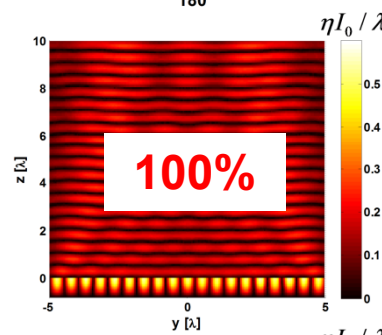
Arxiv:1604.0110100v1



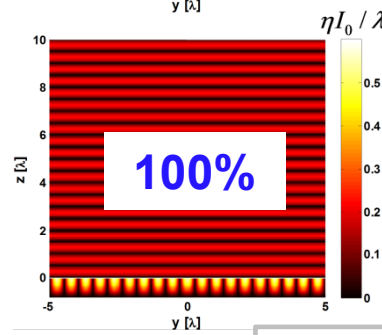
$f = 20\text{GHz}$



**Full-wave
(Discretization)**



Mode purity!



Semianalytical

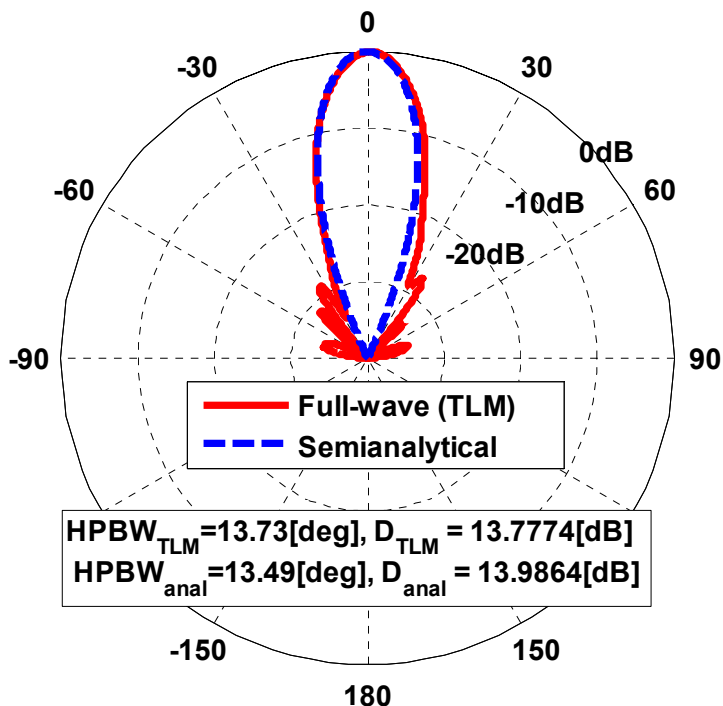
$$d = 0.81\lambda$$

$$L = 10\lambda$$

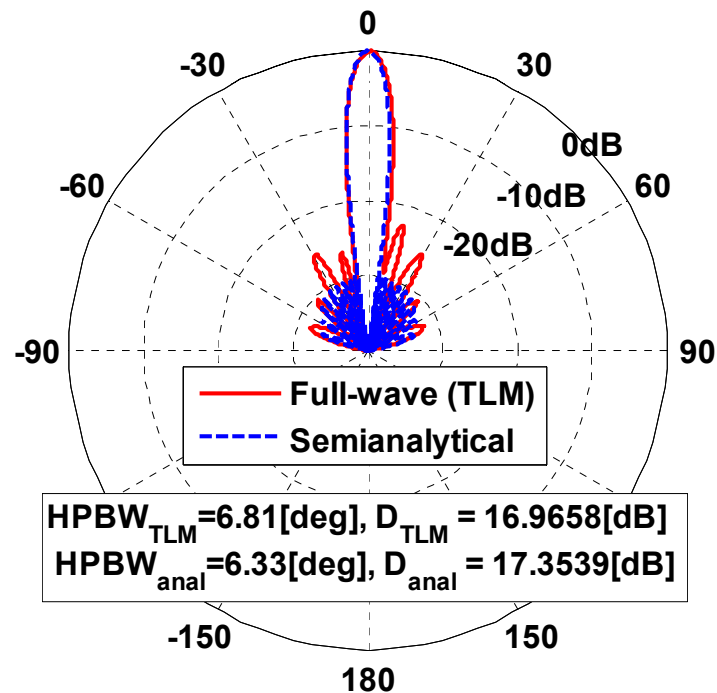
Half the thickness!

Advanced Pattern Control

**Binomial virtual array
($L=10\lambda$)**

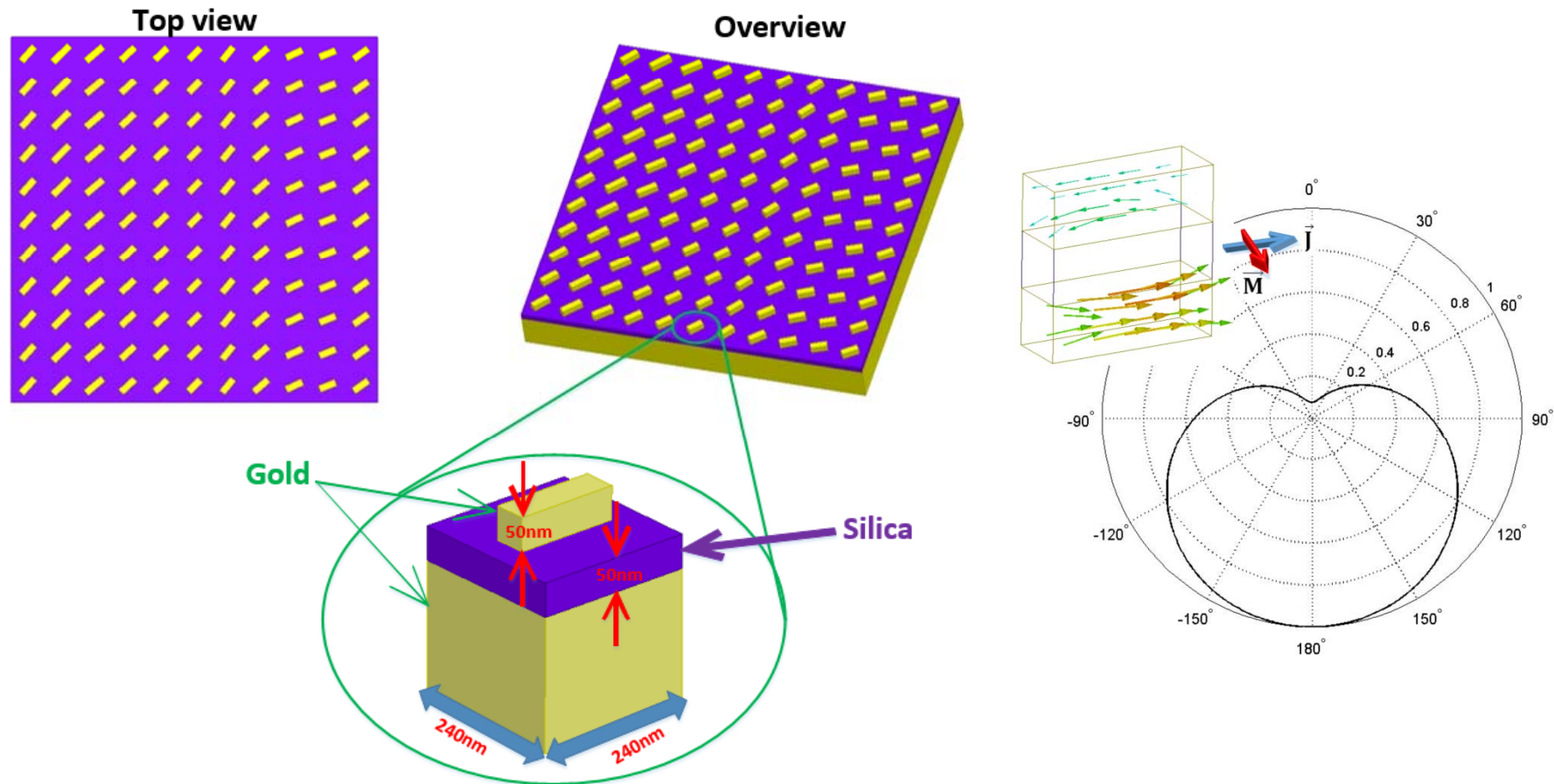


**Chebyshev virtual array
($L=10\lambda$, $SLL=-30dB$)**



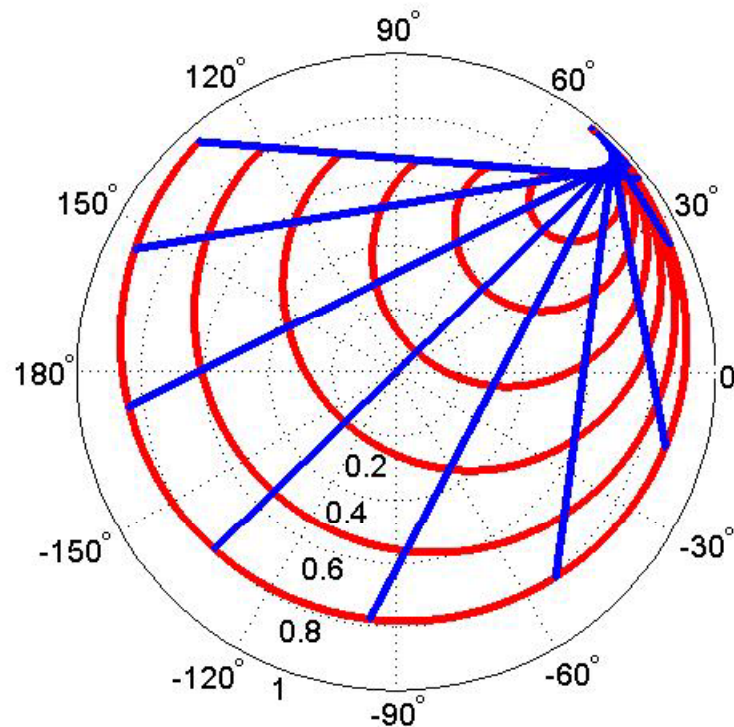
BMS modal refl. coeff.: MANY degrees of freedom!

Optical Huygens' Metasurfaces (complete phase & magnitude control)

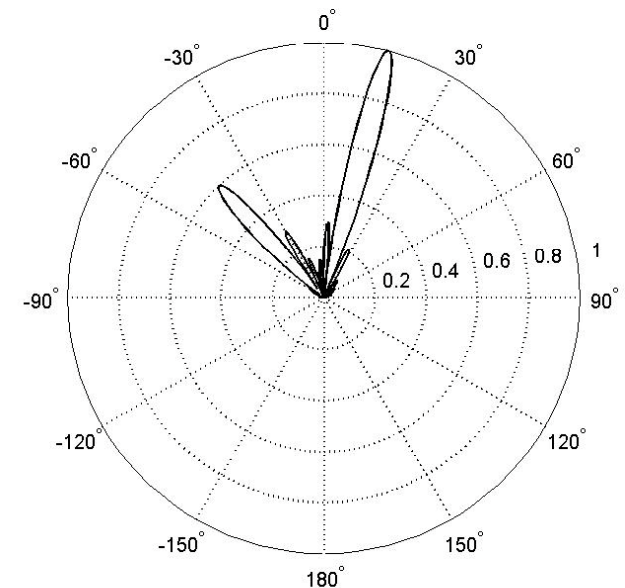
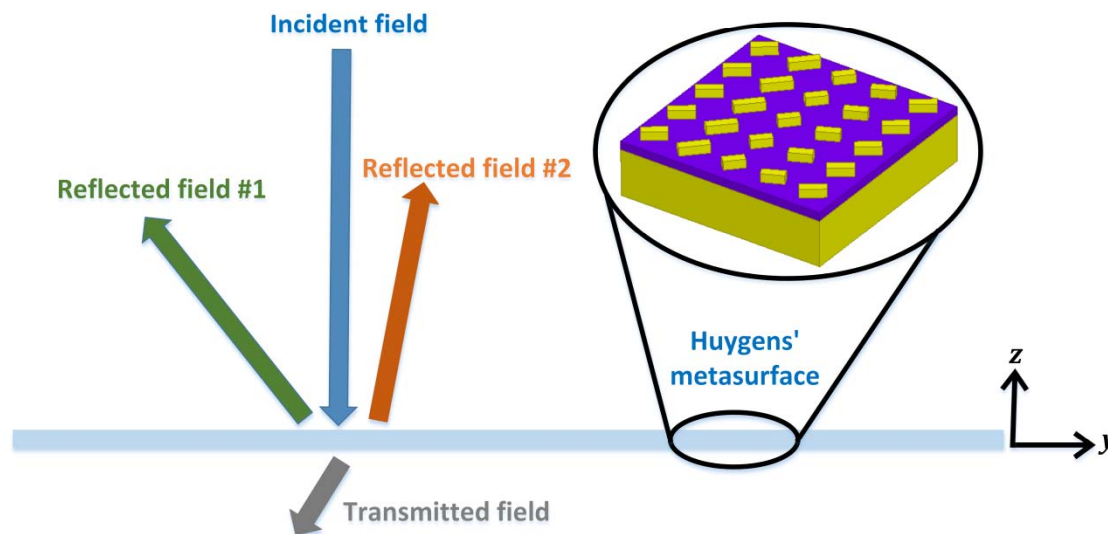


- Each unit-cell simultaneously employs both electric and magnetic resonances and mimics a Huygens' source

Optical Huygens' Metasurfaces (complete phase & magnitude control)

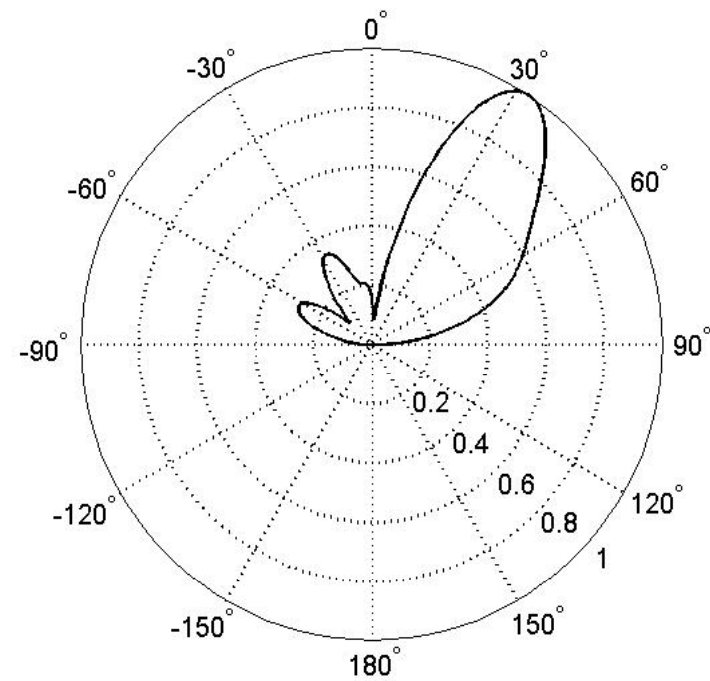
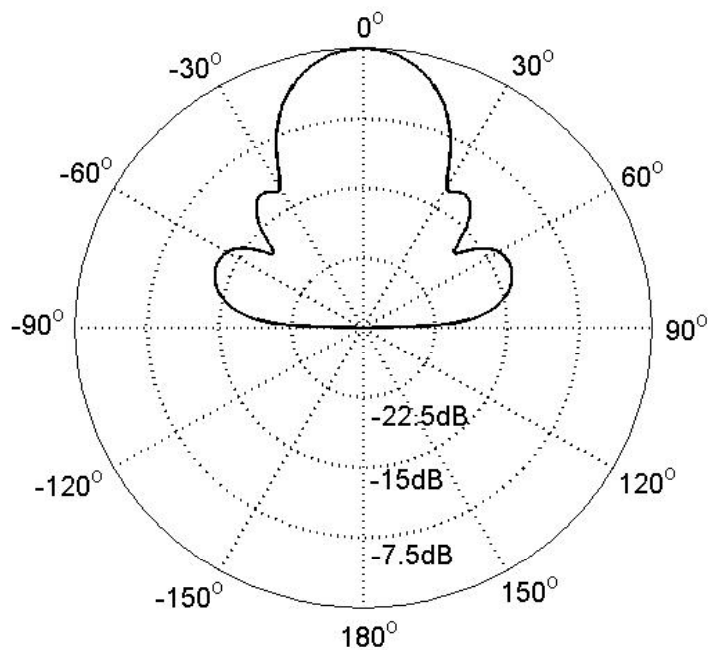


Arbitrarily Reflecting Incident Field: Beam-Splitter



- Able to re-direct incident light at any arbitrary direction
 - Can be extended to the designs of exotic optical reflectarrays and focusing lenses

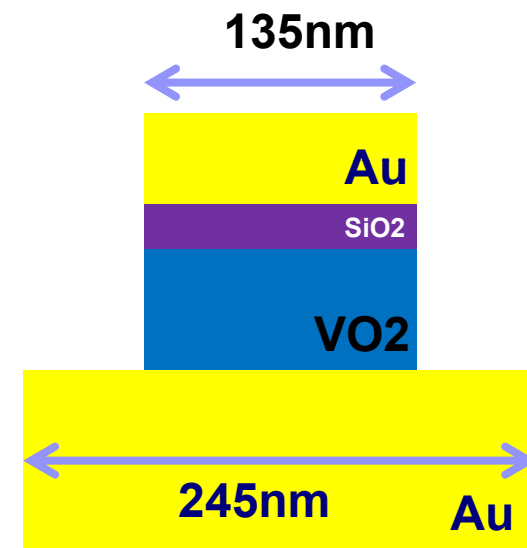
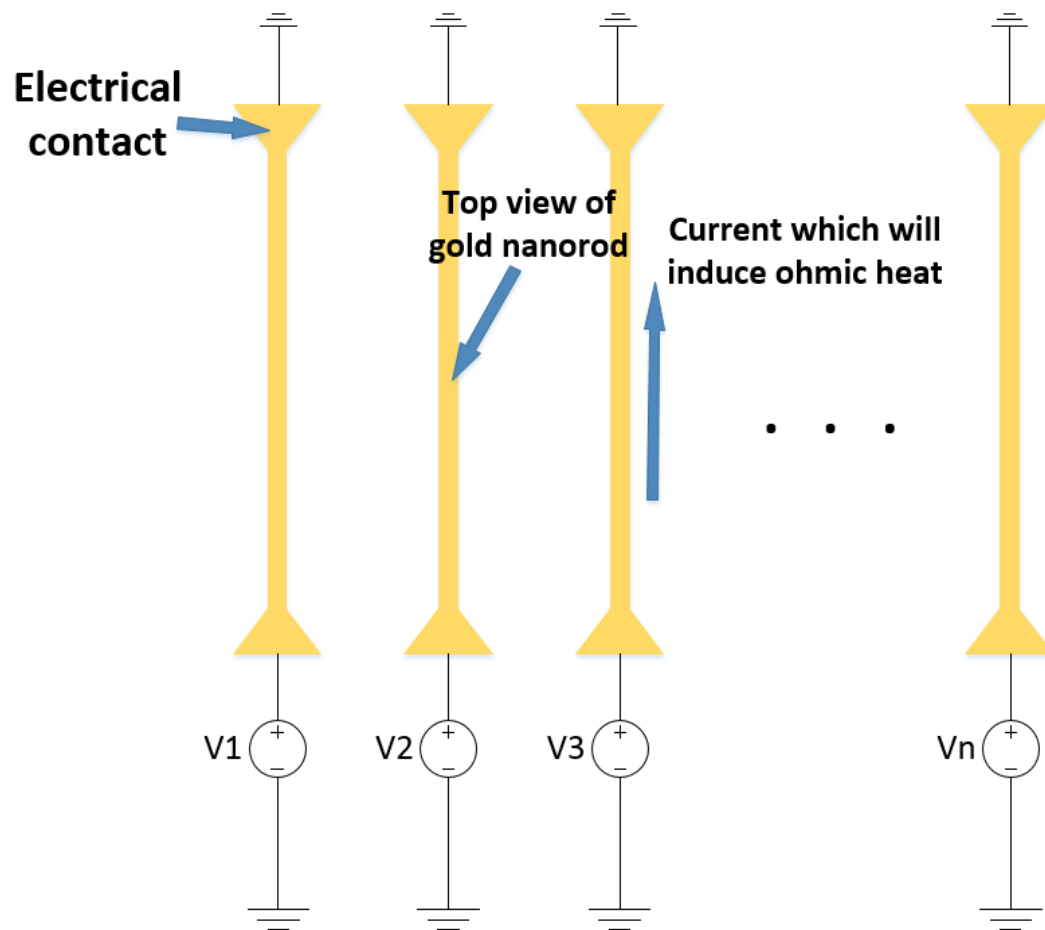
Optical Chebyshev Pattern



Optical Reconfigurable Metasurfaces Using the Phase Transition of VO₂

Top view

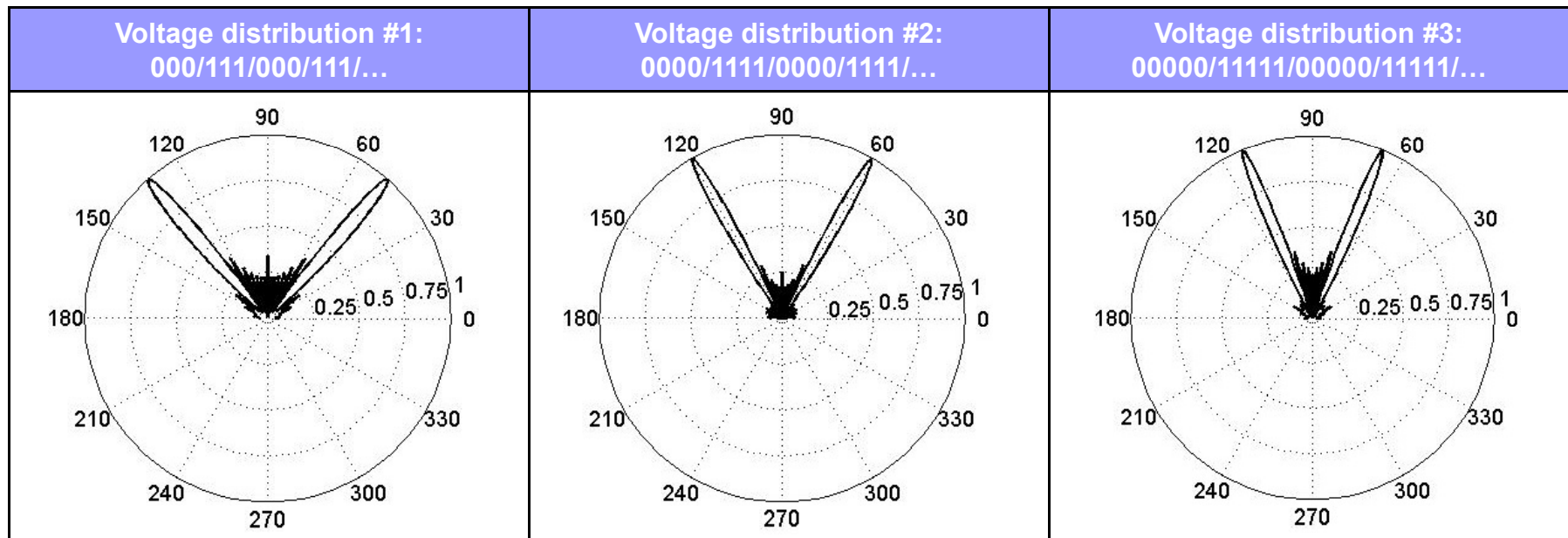
Cross-sectional view: (for one unit cell)



SiO₂ thickness: 10nm
VO₂ thickness: 50nm
Top Au thickness: 30nm

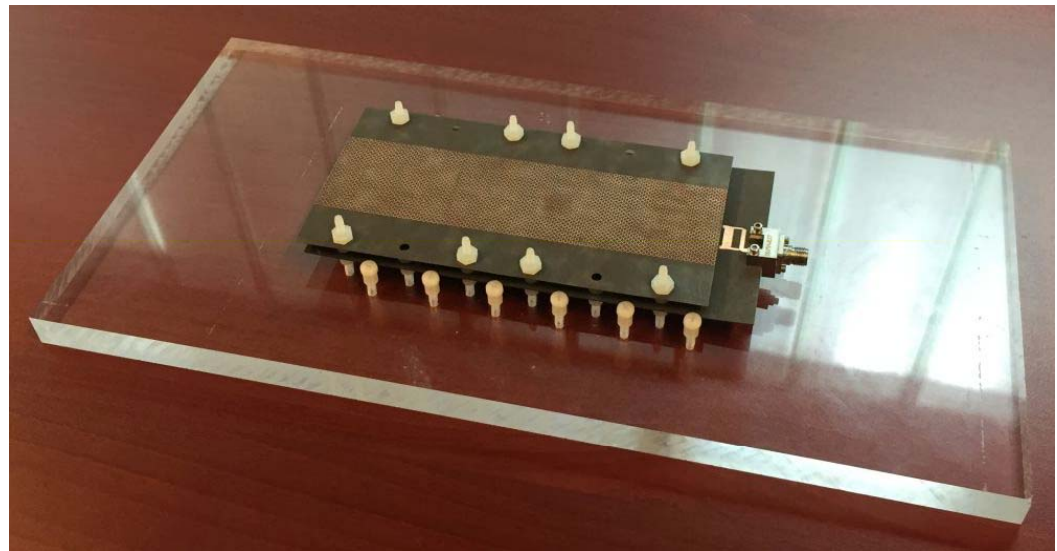
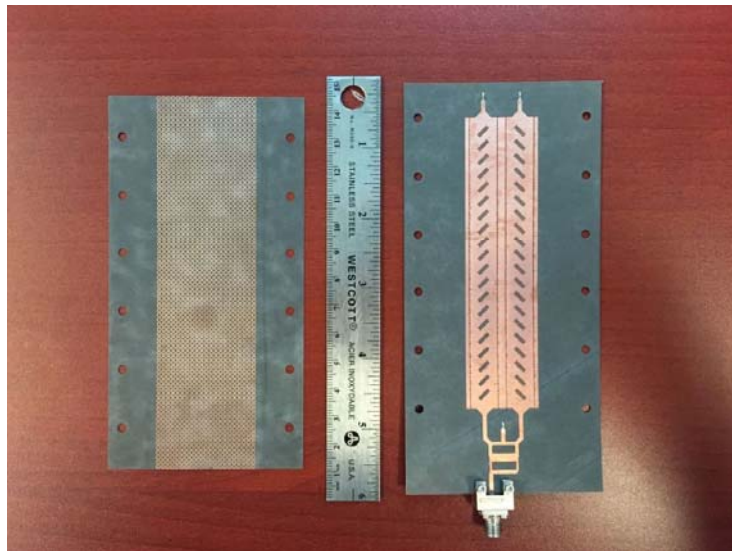
Dynamic manipulation of reflected wavefront

- Dynamic control of the reflected wavefront depending on the digital voltage distribution (i.e., V_n on = 1 and V_n off = 0) on the digital optical metasurface.



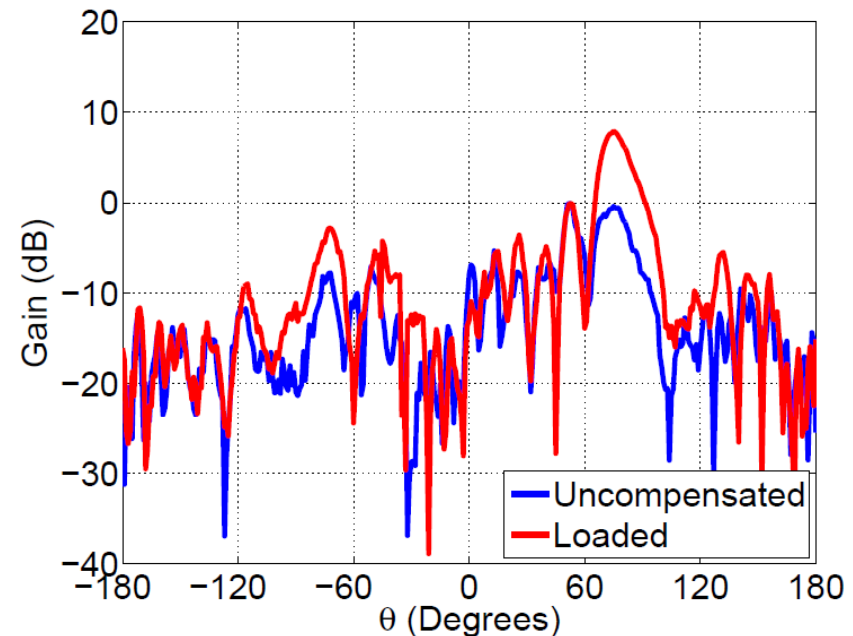
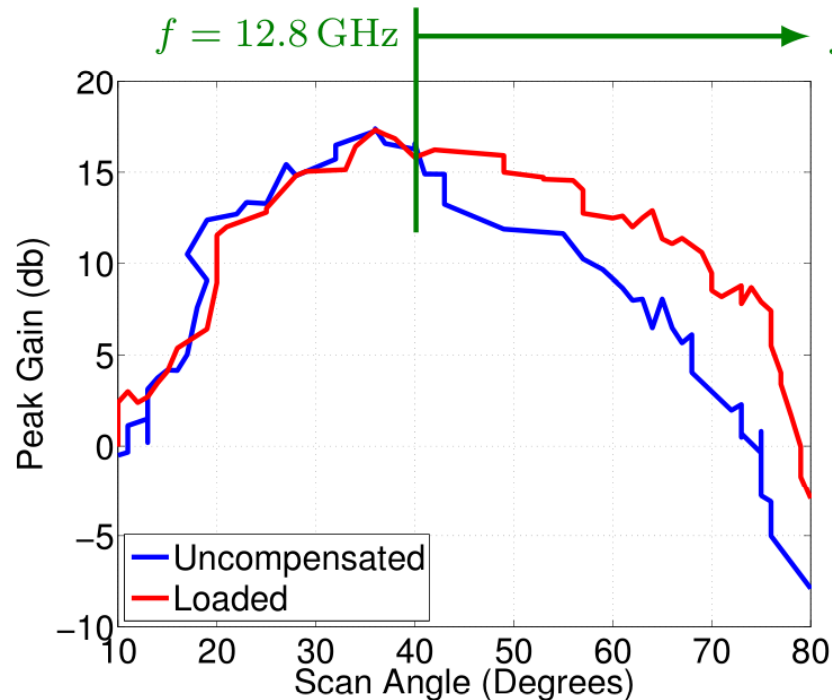
EXTENDING THE SCAN RANGE OF ARRAYS WITH METASURFACES

- Leaky-wave antenna scans beam as a function of frequency
- Etched on Rogers Duroid 5870

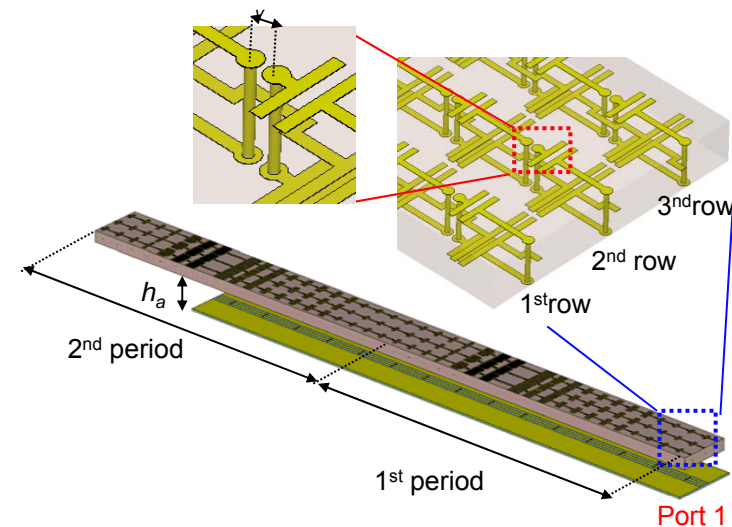
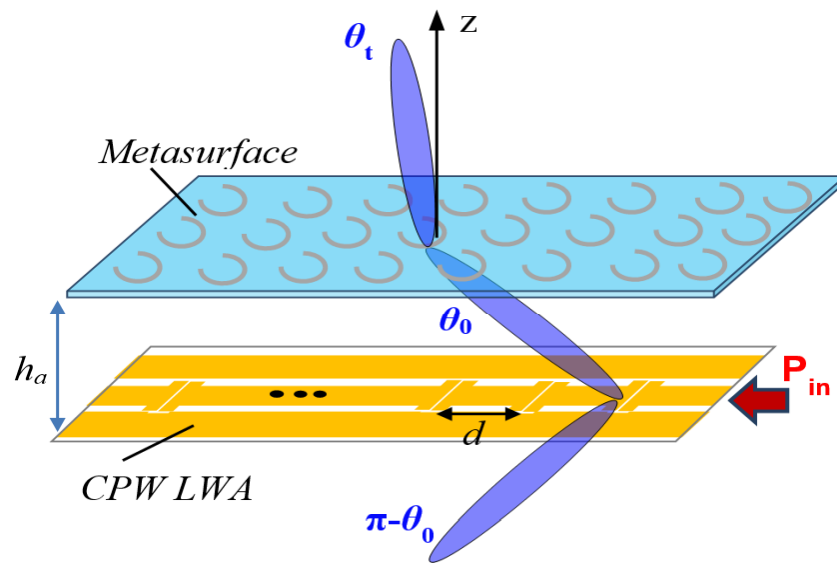


Experimental Validation:

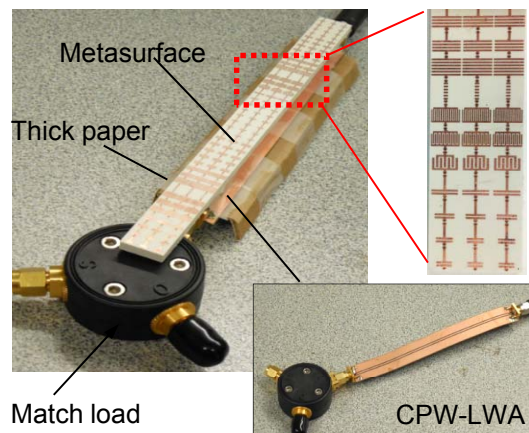
- Gain improvement beyond 45° , as expected
- Remarkable bandwidth
- Minimal impact on cross-polarization levels



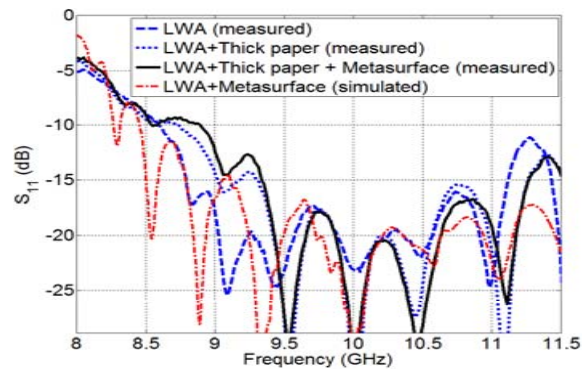
Beam Squinting Reduction of Leaky-Wave Antennas using Huygens' Metasurfaces



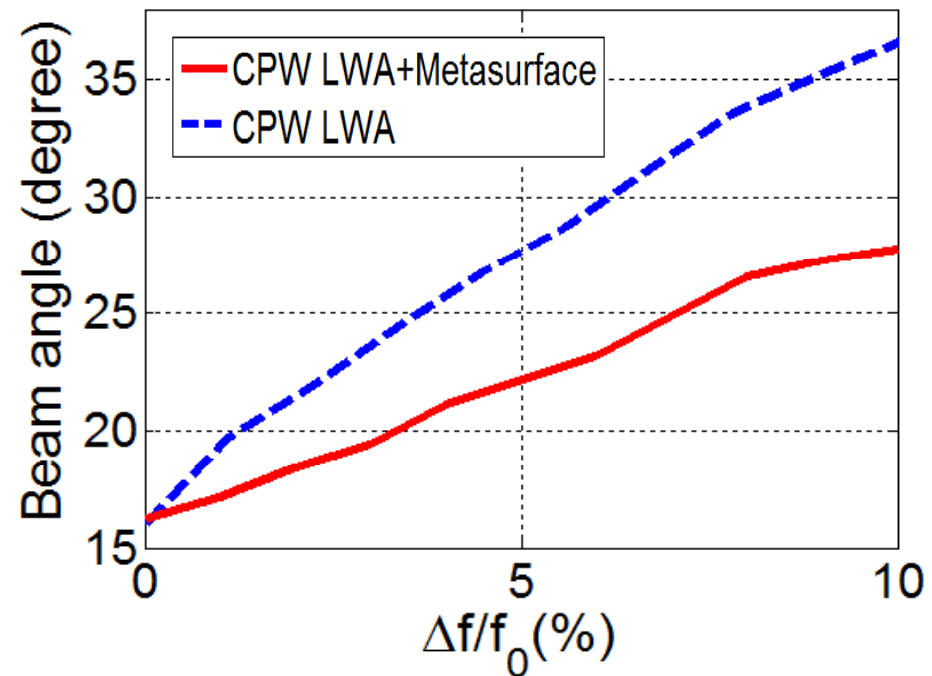
Beam Squinting Reduction of Leaky-Wave Antennas using Huygens' Metasurfaces



(a)



(b)





Advantages of Huygens' Metasurfaces

- Complete control of magnitude, phase and polarization state (including chiral effects)
- Incident field can be a plane-wave, a beam or a nearby source
- Sub-wavelength thin surfaces
- Controlled reflection coefficient
- Microwave, THz or optical implementation possible
- More with active/tuneable metasurfaces!